Excitations and thermodynamics for liquid-helium films*

W. F. Saam
Department of Physics, The Ohio State University, Columbus, Ohio 43210

Milton W. Cole†
Department of Physics, University of Washington, Seattle, Washington 98195

(Received 5 August 1974)

We derive a hydrodynamic theory of the long-wavelength excitations of helium films adsorbed in cylindrical pores and on planar substrates. In the case of cylindrical geometry, the spectrum exhibits an instability for a particular value of the ratio of the film surface radius to the pore radius. This instability condition is shown to coincide with a thermodynamic instability condition determined by the relative magnitude of the surface energy and the energy of interaction with the substrate. Calculated adsorption isotherms show a corresponding hysteresis in good agreement with measured values. We suggest the possibility that the soft modes present for films thinner than the unstable limit mediate an attractive interaction between quasiparticles of a He^3 film adsorbed on the He^4, leading to a new kind of He^3 superfluid. Similar calculations are presented for the spectrum of He^4 on a planar substrate. In this case, as well as in the cylindrical case, surface excitations (ripplons) dominate the thermodynamic properties at low temperature ($T \lesssim 0.1$ K). In this regime the properties are a simple function of the dimensionality of the surface. At higher T, short-wavelength modes contribute, and the results depend in a complicated fashion on the finite dimensions of the system. We discuss the available data, where possible, and suggest further experiments.

I. INTRODUCTION

The properties of liquid films have attracted considerable attention as an application of concepts in statistical mechanics, hydrodynamics, and the physics of adsorption. Helium films have been a particular focus for much of this research because superfluid behavior is modified in a restricted geometry. Although Bose-Einstein condensation is not possible in a film[1] of infinite lateral extent, many experiments have found evidence for superfluidity in films as thin as three atomic layers.[2-4] The nature of this interesting state is an unsolved problem.

In this paper we calculate the excitation spectrum of films using the equations of ideal compressible fluid hydrodynamics. Two kinds of oscillatory modes are found. In one of these, the fluid motion is localized near the liquid-vapor interface. The other is a sound wave, or phonon, involving motion throughout the liquid. For very thin films, this distinction becomes arbitrary, for wavelengths of the "surface" mode may exceed the film thickness. In both cases the motion is affected by boundary conditions at vapor and substrate interfaces with the liquid. Thus the normal modes of the system are sensitive to the particular geometry being considered. We treat here cylindrical and planar geometries, of which the former represents an idealization of the topology of various porous materials.

Atkins was the first to investigate the properties of surface waves in thin films.[5] These oscillatory modes, called third (fourth) sound in the presence (absence) of a free surface have proved valuable in determining the film superfluid density and interaction with the substrate.[3,6-8] Further, more detailed investigation is particularly useful because the thermodynamic properties of helium films are related to the calculated excitations of the system. As the film thickness is decreased, the relative contribution of the surface modes increases, eventually dominating that of the bulk modes. For sufficiently low temperature and small film thickness, the film's properties are determined essentially by the dimensionality of the surface. The criteria governing this simple regime are, and this must be strongly emphasized, quite stringent.

Section II presents the theoretical formalism employed to calculate the excitation spectra and thermodynamic properties of the films. Section III discusses its application to a film adsorbed in a cylindrical pore.[9] Especially dramatic behavior is found in this geometry, for which the surface modes exhibit an instability. Related to adsorption isotherm measurements, this instability and its associated metastability help to resolve a controversy concerning the general problem of films (superfluid or normal) in porous media. Further, the presence of the instability makes credible the existence of a new kind of superfluidity, in the He^3 layer above a He^4 film, for which the attractive interaction between fermions is mediated by excitations of the He^4. Comparisons are made, where possible, to extant experimental results (all in porous Vycor). More reliable comparisons could be made were data available for porous media,

such as Nuclepore filters, where the pore geometry is better known and more easily controlled. Section IV reports calculations for planar geometry. Section V summarizes our results.

II. DYNAMIC AND THERMODYNAMIC EQUATIONS

We begin this section with a discussion of the simplifying assumptions which we will make in order to treat the physics of superfluid He^4 in restricted geometries. The basic approximation used is that the problem may be treated in terms of a model where the mass density ρ varies rapidly over the first few layers of He^4 near the walls, and is uniform with a value approximately equal to the density ρ_0 of bulk He^4 at zero temperature T and zero pressure P elsewhere in the fluid. The first few layers are assumed to be bound so strongly to the walls that they do not participate in superfluid motion, and the remainder of the fluid is assumed to be entirely superfluid at $T=0$. That the first few layers are bound to the substrate and that the superfluid mass increases linearly with coverage as additional layers are added has been confirmed by experiments on superfluid flow in porous Vycor[4] and measurements in thin planar films of the third-sound velocity[3] and the normal-fluid density.[10] The last of these strongly suggests that the bulk normal-fluid density away from the first few layers is probably negligible at $T=0$; we shall take it to be zero. We will simply assume that there is no appreciable normal fluid at a free surface at zero temperature.[11] If there were, this would probably appear in experiments designed to measure surface second sound, and it does not appear to do so.[12] We neglect the small compression of the fluid due to pressure differences existing across free surfaces.

Next, within the context of the model just discussed, we make the premise that the theory of quantum hydrodynamics[13] provides us with an accurate description of the long-wavelength elementary excitations of superfluid He^4 in restricted geometries. More specifically, we assume that the normal modes found from the linearized equations of motion for an ideal zero-temperature fluid in the presence of an external potential (the substrate potential) become, when quantized, the low-lying elementary excitations of the He^4. We shall, for the most part, restrict ourselves to temperatures sufficiently low that more energetic excitations, such as rotons, may be ignored. An exception is made in Sec. IV for the case of planar geometry.

To describe the motion of the bulk we need only the equations for number conservation and superfluid motion. In linear form these are, respectively,[13]

$$\frac{\partial\rho(\vec{r}t)}{\partial t}+\rho_0\vec{\nabla}\cdot\vec{v}_s(\vec{r}t)=0\ , \tag{2.1}$$

$$\frac{\partial\vec{v}_s(\vec{r}t)}{\partial t}+\frac{1}{m_4}\vec{\nabla}\mu(\vec{r}t)=0\ , \tag{2.2}$$

where $\vec{v}_s$ is the superfluid velocity, m_4 is the He^4 atomic mass, and μ is the chemical potential. It is convenient to rewrite (2.2) in terms of the velocity potential $\varphi(\vec{r}t)$ defined by $\vec{v}_s(\vec{r}t)=\vec{\nabla}\varphi(\vec{r}t)$. Thus,

$$\frac{\partial\varphi(\vec{r}t)}{\partial t}+\frac{1}{m_4}\delta\mu(\vec{r}t)=0\ , \tag{2.3}$$

in which $\delta\mu$ is the deviation of μ from its equilibrium value.

The chemical potential is given by[14]

$$\mu(\vec{r}t)=\mu_0(\rho(\vec{r}t))+U(\vec{r})\ , \tag{2.4}$$

where $U(\vec{r})$ is the substrate van der Waals potential and $\mu_0(\rho(\vec{r}t))$ is the bulk He^4 chemical potential at density ρ_0. Neglecting the effect of $U(\vec{r})$ in compressing the liquid, it then follows that

$$\delta\mu(\vec{r}t)=(m_4s^2/\rho_0)[\rho(\vec{r}t)-\rho_0]\ , \tag{2.5}$$

where s is the sound velocity in bulk He^4 at density ρ_0.

Now, for our purposes the content of Eqs. (2.1) and (2.3) is contained in the wave equation which may be combined to give. Using (2.5) we obtain

$$\frac{\partial^2\varphi(\vec{r}t)}{\partial t^2}-s^2\nabla^2\varphi(\vec{r}t)=0\ . \tag{2.6}$$

The boundary conditions to be used with (2.6) are that the normal component of the velocity at any wall (with unit normal $\hat{n}_w$) be zero,

$$\vec{v}_s(\vec{r}_w t)\cdot\hat{n}_w=\vec{\nabla}\varphi(\vec{r}_w t)\cdot\hat{n}_w=0\ , \tag{2.7}$$

and that at a free surface[15]

$$\vec{v}_s(\vec{r}_s t)\cdot\hat{n}_s=\frac{\partial\zeta(\vec{r}_s t)}{\partial t}\ , \tag{2.8}$$

$$\delta P(\vec{r}_s t)=\sigma K(\vec{r}_s t)\ . \tag{2.9}$$

In these equations $\hat{n}_s$ is a unit outward normal from the surface, $\zeta(\vec{r}_s t)$ is the outward displacement of the surface from its equilibrium position, $K(\vec{r}_s t)$ is the sum of the two inverse radii of curvature at a point $\vec{r}_s$ on the surface, σ is the surface tension,[16] and $\delta P(\vec{r}_s t)$ is the pressure discontinuity across the interface. We use subscripts s and w to indicate that quantities are evaluated at a free surface or a wall, respectively. In the situations to be considered in later sections $K(\vec{r}_s t)$ will have the form

$$K(\vec{r}_s t)=K_0+K_1^{\mathrm{op}}\zeta(\vec{r}_s t)\ , \tag{2.10}$$

where K_0 is the equilibrium curvature and K_1^{op} is, in general, a linear differential operator acting on

$\zeta(\vec{r}_s t)$.

The boundary conditions at a free surface can be combined into a single equation if we note that [see (2.4)]

$$\delta P(\vec{r}_s t) = P_0 + (\rho_0/m_4)\,\delta\mu_0(\rho(\vec{r}_s t)) = P_0 + (\rho_0/m_4)[\delta\mu(\vec{r}_s t) - \nabla U(\vec{r}_s t)\cdot\hat{n}_s \zeta(\vec{r}_s t)]\,. \tag{2.11}$$

Here, $P_0 = \sigma K_0$ is the equilibrium pressure discontinuity across the free surface. Combining (2.3) and (2.8)–(2.11) we arrive at a single equation expressing the free surface boundary condition:

$$\frac{\partial^2 \varphi(\vec{r}_s t)}{\partial t^2} = -[g(\vec{r}_s) + (\sigma/\rho_0) K_1^{op}]\,\vec{\nabla}\varphi(\vec{r}_s)\cdot\hat{n}_s\,. \tag{2.12}$$

Here,

$$g(\vec{r}_s) \equiv +(1/m_4)\,\vec{\nabla} U(\vec{r}_s)\cdot\hat{n}_s\,. \tag{2.13}$$

The normal-mode problem is stated in its most concise form by Eqs. (2.6) and (2.12). Labeling a general mode by subscript l and assuming $\varphi_l(\vec{r}t) = \varphi_l(\vec{r})\,e^{-i\omega_l t}$, these equations become

$$\nabla^2\varphi_l(\vec{r}) + (\omega_l^2/s^2)\,\varphi_l(\vec{r}) = 0 \tag{2.14}$$

$$[g(\vec{r}_s) + (\sigma/\rho_0) K_1^{op}]\,\vec{\nabla}\varphi_l(\vec{r}_s)\cdot\hat{n}_s = \omega_l^2\,\varphi_l(\vec{r}_s)\,. \tag{2.15}$$

This set of classical field equations may be quantized in the usual way,[17] leading to a Hamiltonian

$$H = \sum_l \hbar\omega_l a_l^\dagger a_l\,, \tag{2.16}$$

where $a_l^\dagger$ and a_l are creation and annihilation operators for quanta in the lth mode, and the zero-point energy has been omitted. It is expected that the long-wavelength excitations found in this way will be well defined. For example, it has been shown[18] that ripplons on a planar surface of bulk He^4 are not significantly damped for wave numbers less than a few inverse atomic spacings.

Given (2.16), the thermodynamics of a given system is straightforward. For example, the energy, referred to the ground-state energy, is simply

$$E = \sum_l \hbar\omega_l f(\beta\hbar\omega_l)\,, \tag{2.17}$$

where $\beta = 1/k_B T$, and $f(x) = (e^x - 1)^{-1}$ is the Bose distribution function. The normal-fluid density is defined in terms of the momentum $\vec{P}$ associated with the normal-fluid velocity $\vec{v}_n$. In the frame where $\vec{v}_s = 0$,

$$\vec{P} = \sum_l \vec{P}_l f(\beta(\hbar\omega_l - \vec{P}_l\cdot\vec{v}_n)) \approx -\beta\sum_l \vec{P}_l\,\vec{P}_l\cdot\vec{v}_n f'(\beta\hbar\omega_l)\,. \tag{2.18}$$

Here $\vec{P}_l$ is the momentum associated with the lth mode. Examples will be worked out in later sections.

To calculate both the excitation spectrum and the thermodynamic properties of the adsorbate, we must know the interaction between particles of the film and the substrate. If the forces are of the van der Waals type, as we assume here, they are related to the interaction between fluctuations of the electric polarization of the film and those of the substrate. Dzyaloshinski *et al.*[19] have derived an expression for this interaction in terms of the frequency-dependent dielectric functions of the two media. In the case of a planar substrate and a weakly polarizable adsorbate, for example He, these authors obtain a relation between the chemical potential of the film $\mu(D)$ and that of the bulk liquid μ_0,

$$\mu(D) - \mu_0 = U(D)\,, \tag{2.19}$$

where $U(D)$ is the interaction between a single adsorbate particle and the substrate, separated by a distance D. For $D \ll \lambda_c$, a characteristic wavelength in the particle's adsorption spectrum, the interaction takes the form

$$U(D) = -\alpha/D^3\,, \tag{2.20}$$

while in the retardation regime ($D \gg \lambda_c$), U varies as D^{-4}. This behavior has been seen in a number of He adsorption experiments. Sabisky and Anderson[20,21] have verified the prediction of the coefficient α for $D \gtrsim 10$ Å films on a variety of substrates. It should be noted that Eq. (2.19) implicitly assumes that the substrate provides a weak slowly varying perturbation on a film that is otherwise identical to the bulk liquid. For sufficiently thin films, this is obviously an oversimplification. Our approach for general substrate geometries will be to use (2.4) with $U(\vec{r})$ determined by assuming that it is given by a sum of pair interactions of the form $-c/r^6$ with the substrate atoms, taken to have number density n_s. Explicitly,

$$U(\vec{r}) = -n_s c \int d^3r'\,|\vec{r} - \vec{r}'|^{-6}\,. \tag{2.21}$$

Close to the substrate this reduces to the planar result (2.20), with $\alpha = \frac{1}{6}\pi n_s c$. For α we take the calculated planar values. While not equivalent, except for strictly planar geometry, to the more exact procedure of Dzyaloshinski *et al.*,[19] this approach provides a simple semiquantitiative description of the film-substrate interaction. We next embark upon a detailed analysis of the case where the helium is confined in a cylindrical pore, the situation approximately obtaining in porous Vycor glass.

III. CYLINDRICAL GEOMETRY

Measured properties of helium in porous Vycor glass have usually been interpreted in terms of a

model where the solid glass is permeated by long, straight, cylindrical holes all having approximately the same radius. The pores occupy approximately 30% of the total volume, and their mean radius is of order 30 Å.[22] These results were obtained by analyzing sorption isotherm data with BET (Brunauer, Emmet, and Teller[23]) theory. The theory to be described below, which we feel to be based on rather more sound physical ideas, leads to essentially the same numbers. Further, we provide a new explanation, based on a surface-mode instability,[9] of the phenomenon of hysteresis commonly observed in sorption experiments in porous materials.[24] By making a simple assumption about the nature of the pore radius distribution we obtain sorption isotherms in rather good agreement with the data of Brewer and Champeney,[25] including the hysteresis loop. The BET theory does not account for hysteresis. We believe that the agreement could be considerably improved given more detailed knowledge of the pore-size distribution, and we suggest how some specific experiments could be used to obtain such knowledge.

Our analysis begins with discussions of the modes and resultant thermodynamics for two cases, first that of filled pores, and secondly for partially filled pores. An important result of this discussion is the clarification of the nature of size effects on the thermodynamics of helium in Vycor. At very low temperatures, degrees of freedom associated with directions transverse to the cylinder axis become frozen out so that the system becomes effectively one dimensional. This occurs at different temperatures depending on whether or not the pores are filled, but in neither case is the one-dimensional limit valid for $T > 0.1$ K. For $0.1 < T < 1.0$ K, one cannot expect comparisons of data with the one-dimensional limit, or with the three-dimensional bulk He^4 results to be particularly useful. Above 1 K, but below the transition temperature[26] for the system, the three-dimensional limit should obtain, assuming the rotons are not altered by the restricted geometry. The last subsection is devoted to a detailed discussion of sorption of helium in porous Vycor. Throughout, we make comparisons with the available experimental data.

A. Filled pores

In this case we require only Eqs. (2.8) and (2.14) of the previous section. Assuming a solution of the form

$$\varphi_{km}(r, \theta, z) = f_{km}(r)\, e^{i(kz+m\theta)} , \tag{3.1}$$

in terms of the variables r, θ, and z appropriate to cylindrical symmetry, (2.14) becomes

$$\frac{d^2 f_{km}}{dr^2} + \frac{1}{r}\frac{df_{km}}{dr} + \left(\frac{\omega^2}{s^2} - k^2 - \frac{m^2}{r^2}\right) f_{km} = 0 . \tag{3.2}$$

The boundary condition (2.8) is simply

$$\left.\frac{\partial f_{km}}{\partial r}\right|_{r=R} = 0 , \tag{3.3}$$

where R is the effective pore radius (allowing for the layers bound to the Vycor surface). The allowed solutions to (3.2) and (3.3) are Bessel functions $f_{km}(r) = J_m(qr)$ (Ref. 27) where

$$q^2 = \omega^2/s^2 - k^2 , \tag{3.4}$$

and q is determined by the condition $J'_m(qR) = 0$. Defining the lth zero of $J'_m(x)$ as x_{ml}, the eigenvalues are then

$$\omega^2_{kml} = s^2(k^2 + x^2_{ml}/R^2) . \tag{3.5}$$

The allowed values of k are determined by periodic boundary conditions along the axis of the cylinder. Since $J_m(x) = (-1)^m J_{-m}(x)$, the $\pm m$ modes are degenerate. No mode exists for $l = 1$, $m \geq 2$, because then $x_{m1} = 0$ and $J_m(0) = 0$ imply that $f_{km} = 0$ everywhere.

Given ω_{kml}, we can calculate the thermodynamic properties of He^4 via (2.17) and (2.18). The energy is given by

$$E = L\int_{-\infty}^{\infty}\frac{dk}{2\pi}\left(\sum_{m=-1}^{+1}\hbar\omega_{km1} f(\hbar\beta\omega_{km1}) + \sum_{m=-\infty}^{\infty}\sum_{l=2}^{\infty}\hbar\omega_{kml} f(\beta\hbar\omega_{kml})\right) . \tag{3.6}$$

The detailed evaluation of (3.6) is worthwhile and tractable only in the case of low temperatures, where $k_B T \ll \hbar s R$ (i.e., $T < 0.1$ K for $R \approx 30$ Å). Define

$$E_{ml} = L\int_{-\infty}^{\infty}\frac{dk}{2\pi}\hbar\omega_{kml} f(\beta\hbar\omega_{kml}) . \tag{3.7}$$

Then, as $x_{01} = 0$,

$$E_{01} = 2L\int_0^{\infty}\frac{dk}{2\pi}\frac{\hbar s k}{e^{\beta\hbar s k} - 1} = \frac{\pi L}{6\hbar s\beta^2} . \tag{3.8}$$

Since $x_{ml} \neq 0$ for the remaining terms in (3.6), all other E_{ml} have the form

$$E_{ml} = 2L\int_0^{\infty}\frac{dk}{2\pi}\frac{\hbar\omega_{kml}}{e^{\beta\hbar\omega_{kml}} - 1} = \frac{L}{\pi}\frac{1}{\beta^2\hbar s}\int_{z_{ml}}^{\infty}\frac{z^2}{(z^2 - z^2_{ml})^{1/2}}\frac{dz}{e^z - 1} . \tag{3.9}$$

In the limit that $z_{ml} \equiv \beta\hbar s x_{ml}/R \gg 1$, the integral can be evaluated in terms of the derivative $K'_1(x)$ of the modified Bessel function $K_1(x)$. We find:

$$E_{ml} = -(L/\pi)(1/\beta^2\hbar s)\, z^2_{ml} K'_1(z_{ml}) . \tag{3.10}$$

Finally, using the large argument expansion of K'_1,

$$E_{ml} \approx (L/\pi)(1/\beta^2\hbar s)\sqrt{\tfrac{1}{2}\pi}\,(z_{ml})^{3/2} e^{-z_{ml}} , \tag{3.11}$$

for $z_{ml} \gg 1$.

Now, if $R \approx 30$ Å, $z_{ml} = 0.6\, x_{ml}/T$. Further, the first few x_{ml}'s are $x_{11} = 1.84$, $x_{22} = 3.05$, $x_{02} = 3.83$, and $x_{32} = 4.20$. Therefore, it is clear from (3.8) and (3.11) that for $T \sim 1$ K all of the terms in (3.6) will give significant contributions. Further, since the effective level spacing divided by $k_B T$ is of the order of the difference between successive z_{ml}'s, i.e., of order unity for $T \sim 1$ K, the sum over m and l in (3.6) cannot be replaced by an integral. It follows that the energy, even at 1 K, may not be approximated by that for phonons in an infinite system—the system does not behave as if it were three dimensional.

Let us assume that T is sufficiently low that we need only retain the leading term of the type (3.11). Then,

$$E \approx (\pi L/6\hbar s\beta^2)\left[1 + (6/\pi^{3/2}2^{1/2})(z_{11})^{3/2} e^{-z_{11}}\right] . \tag{3.12}$$

The ratio of the specific heat c to that of three-dimensional He^4, c_{bulk}, is (neglecting the roton contribution to c_{bulk})

$$\frac{c}{c_{\text{bulk}}} = \frac{5}{2\pi^2}\left(\frac{\hbar s\beta}{R}\right)^2 \left(1 + \frac{6}{(2\pi)^{3/2}}\, z_{11}^{3/2}(\tfrac{1}{2} + z_{11}) e^{-z_{11}}\right) . \tag{3.13}$$

This result has several interesting features. First, even for $T = 0.3$ K, the second term in brackets is ~ 0.25. The one-dimensional limit is reached for $T \sim 0.1$ K where the second term is of order 10^{-2}. Second, for $T \lesssim 0.1$ K, $c/c_{\text{bulk}} \approx 80/(RT)^2$, if R is expressed in Å, indicating considerable enhancement for small R and T.

We remark in passing that if the roton part of c_{bulk} is included, c/c_{bulk} becomes of order one for $T \sim 0.7$ K. Therefore, for temperatures much higher than this, the system will be bulk-like if the rotons are not affected by the geometrical restrictions. This has been observed by Brewer.[1]

Recent data of Tait and Reppy[28] give full pore heat capacities down to temperatures slightly less than 0.1 K. However, at these temperatures they obtain a T^2 contribution from the solid helium near the Vycor walls which is several times larger than our result. A definitive comparison between our result ($c \sim T$) and experiment could only be made at even lower temperatures.

The momentum associated with normal-fluid flow along the axis of the cylinder can be found from (2.18). For temperatures sufficiently low that we need only account for the $m = 0$, $l = 1$ modes,

$$P = -2\,\beta v_n L \int_0^\infty \frac{dk}{2\pi}\,(\hbar k)^2 f'(\beta\hbar s k) = \frac{\pi(k_B T)^2}{3\hbar s^3}\, L v_n . \tag{3.14}$$

Consequently, the normal mass per unit length ν_n, defined by $P = L\nu_n v_n$, is

$$\nu_n = \pi(k_B T)^2/3\hbar s^3 . \tag{3.15}$$

The quantity of more direct experimental interest is the normal mass per unit volume

$$\rho_n \equiv \nu_n/\pi R^2 = (k_B T)^2/3\hbar s^3 R^2 . \tag{3.16}$$

Recent measurements[29] down to temperatures slightly below 0.1 K, in Vycor, confirm the temperature dependence exhibited in (3.16), but for $R \approx 30$ Å, our coefficient of T^2 is several orders of magnitude too small. We take this to be an indication that the single cylindrical pore approximation for Vycor is not a good one. The discrepancy can perhaps be accounted for by replacing s in (3.16) by a geometrically averaged velocity as discussed in Ref. 30. For completeness, we quote the fourth-sound velocity c_4, which can easily be worked out from (3.8) and (3.16). One finds

$$c_4^2 = \rho_s\left(\frac{\partial\mu}{\partial\rho}\right)_S = \left[1 + \left(\frac{W}{2} - 1\right)\frac{\rho_n}{\rho_0}\right] s^2 , \tag{3.17}$$

where $\rho_s \equiv \rho_0 - \rho_n$, S is the entropy, and $W \equiv (\rho_0^2/s)\,\partial^2 s/\partial\rho_0^2 \approx 5.5$.

B. Partially filled pores

Here we examine the situation where the helium fills the space $a \le r \le R$, there being a free surface at $r = a$. We begin with a discussion of the possible modes.

1. Modes

For the case at hand, Eq. (2.15) takes the form

$$\left[-g(a) + \frac{\sigma}{\rho_0 a^2}\left(1 + a^2\,\frac{\partial^2}{\partial z^2} + \frac{\partial^2}{\partial\theta^2}\right)\right]\frac{\partial\varphi(r,\theta,z)}{\partial r}\bigg|_{r=a} = \omega^2\varphi(a,\theta,z) . \tag{3.18}$$

Assuming a solution like (3.1), (2.14) again turns into (3.2), while (3.18) becomes

$$\left(-g(a) + \frac{\sigma}{\rho_0 a^2}\,(1 - a^2k^2 - m^2)\right)\frac{\partial f_{km}(r)}{\partial r}\bigg|_{r=a} = \omega^2 f_{km}(a) . \tag{3.19}$$

There are several subcases to consider here according to the sign of $k^2 - \omega^2/s^2$.

(a) Ripplons, $l^2 \equiv k^2 - \omega^2/s^2 > 0$. Solutions to (3.2) have the form

$$f_{km}(r) = I_m(lr) - A_m(lR)K_m(lr) , \tag{3.20}$$

where I_m and K_m are modified Bessel functions. The boundary condition (2.7) leads immediately to

$$A_m(lR) = I_m'(lR)/K_m'(lR) , \tag{3.21}$$

while the combination of (3.19) and (3.20) yields

$$\omega^2 = \left(-g(a) + \frac{\sigma}{\rho_0 a^2}\,(1 - m^2 - k^2a^2)\right) \times l\,\frac{I_m'(la) - A_m(lR)K_m'(la)}{I_m(la) - A_m(lR)K_m(la)} . \tag{3.22}$$

This equation, together with the above definition of

l, determines the allowed values of ω for given k and m. In general, the solutions have to be found by numerical means. However, for low temperatures and small R, considerable simplification occurs in that one may use the small-argument limits for the Bessel functions in (3.22). Thus, we assume $lR \ll 1$, which, from the definition of l, is equivalent to $kR \ll 1$, i.e., $k \ll (30\ \text{Å})^{-1}$ in Vycor. We look at special cases:

(i) $m = 0$, $lR \ll 1$. Here (3.22) reduces to

$$\omega^2 = [g(a) - (\sigma/\rho_0 a^2)(1 - k^2 a^2)]\, \tfrac{1}{2} l^2 a [(R/a)^2 - 1] . \tag{3.23}$$

Since $l^2 > 0$, $R > a$, and $g(a) > 0$ (as will be shown below), the frequency will become imaginary and the mode unstable for $k \to 0$, unless

$$g(a) > \sigma/\rho_0 a^2 . \tag{3.24}$$

Because this is a long-wavelength instability,[31] one might expect that (3.24) can also be derived from thermodynamic arguments. That this is the case will be demonstrated further on. Using the definition $l^2 = k^2 - \omega^2/s^2$, we may solve (3.23) for the eigenfrequencies, obtaining

$$\omega = c_0 k [(1 + k^2/k_0^2)^{-1} + c_0^2/s^2]^{-1/2} , \tag{3.25a}$$

$$c_0^2 = \tfrac{1}{2}[a g(a) - \sigma/\rho_0 a][(R/a)^2 - 1] , \tag{3.25b}$$

$$k_0^2 = \rho_0 g(a)/\sigma - a^{-2} . \tag{3.25c}$$

One has, in addition,

$$l^2 = k^2/[1 + (c_0^2/s^2)(1 + k^2/k_0^2)] . \tag{3.26}$$

Note that the modes described by (3.25) and (3.26) continue to exist in the limit of an incompressible fluid (i.e., $s^2 \to \infty$). This is one way of seeing that the modes are properly identified as surface modes, or ripplons. A perhaps more general approach is to demonstrate that the usual ripplon dispersion relation emerges from (3.22) in the appropriate limit. Consider the case of a thick film whose inner surface has a curvature large compared to the wavelengths of the modes. Then $lR \to \infty$, and $m \sim ka \gg 1$. In this limit the properties of modified Bessel functions yield $A_m(lR) \to -\infty$, and

$$K_m'(la)/K_m(la) \approx -(1 + m^2/l^2 a^2)^{1/2} .$$

Consequently, (3.22) becomes

$$\omega^2 = (\sigma/\rho_0)(k^2 + m^2/a^2)(l^2 + m^2/a^2)^{1/2} . \tag{3.27}$$

Defining $p^2 = k^2 + m^2/a^2$ and $\kappa^2 = l^2 + m^2/a^2$, (3.27) and the definition $l^2 = k^2 - \omega^2/s^2$ may be written, respectively, as $\omega^2 = (\sigma/\rho_0) p^2 \kappa$ and $\kappa^2 = p^2 - \omega^2/s^2$. These later relations constitute the well-known dispersion relation[13] for ripplons in an infinite compressible fluid with a planar free surface.

(ii) $m \geq 1$, $lR \ll 1$. Here (3.22) reduces to

$$\omega^2 = \left(g(a) + \frac{\sigma}{\rho_0 a^2}(m^2 + k^2 a^2 - 1)\right) \frac{m}{a} \left(\frac{(R/a)^{2m} - 1}{(R/a)^{2m} + 1}\right) . \tag{3.28}$$

Because of the requirement $l^2 > 0$, these modes do not exist unless

$$l^2 = (k^2 - k_m^2)[1 - m b_m \sigma/\rho_0] > 0 , \tag{3.29a}$$

where

$$k_m^2 = m b_m [g(a) + (\sigma/\rho_0 a^2)(m^2 - 1)](1 - m b_m \sigma/\rho_0)^{-1} , \tag{3.29b}$$

and

$$b_m \equiv (1/a s^2)[(R/a)^{2m} - 1]/[(R/a)^{2m} + 1] .$$

(b) Phonons, $q^2 \equiv \omega^2/s^2 - k^2 > 0$. Solutions to (3.2) possess the form

$$f_{km} = J_m(qr) - B_m(qr)\, Y_m(qr) , \tag{3.30}$$

where $B_m(qr)$ as determined by (2.7) is

$$B_m(qR) = J_m'(qR)/Y_m'(qR) . \tag{3.31}$$

The eigenvalue relation becomes

$$\omega^2 = q[-g(a) + (\sigma/\rho_0 a^2)(1 - m^2 - k^2 a^2)] \times \frac{J_m'(qa) - B_m(qR)\, Y_m'(qa)}{J_m(qa) - B_m(qR)\, Y_m(qa)} . \tag{3.32}$$

As was the case for ripplons, several cases are possible:

(i) $m = 0$, $qR \ll 1$. After a bit of algebra in which (3.31), $q^2 = \omega^2/s^2 - k^2$, and the small-argument limits of the Bessel functions are employed, one arrives at

$$q^2 = -k^2/(1 + \gamma_k) , \tag{3.33}$$

where

$$\gamma_k = (a/2s^2)[g(a) - (\sigma/\rho_0 a^2)(1 - k^2 a^2)] . \tag{3.34}$$

The ripplon stability condition (3.24) requires that $\gamma_k > 0$. Consequently, (3.33) violates the requirement $q^2 > 0$; the $m = 0$ phonons do not exist in the limit $ka \ll 1$ (in essence, their place has been taken by the $m = 0$ ripplons).

(ii) $m \geq 1$, $qR \ll 1$. A similar development gives an expression for ω^2 identical to (3.28), subject to the requirement

$$q^2 = (k_m^2 - k^2)(1 - m b_m \sigma/\rho_0 a^2) > 0 . \tag{3.35}$$

Since k_m and b_m approach zero in the limit $s^2 \to -\infty$, these modes disappear in the approximation that the fluid is incompressible.

2. *Thermodynamics*

For low temperatures only the low-frequency modes contribute to the thermodynamics. In particular, since all the modes discussed above, with the exception of the $m = 0$ ripplons, possess a gap as $k \to 0$ (i.e., ω approaches a non-zero constant

as $k \to 0$), the ripplons dominate the thermal properties. It will be seen later that, for interesting values of a, $g(a)$ is of the same order of magnitude as $\sigma/\rho_0 a^2$ [this argument breaks down too near the instability defined in (3.24)]. Hence, from (3.25b), $c_0^2/s^2 \sim \sigma/\rho_0 = 0.46/a$ if a is expressed in Å. Further, $k_0 \sim 1/a$. Consequently, at sufficiently low temperatures, $\omega = c_0 k$ for the ripplons suffices to calculate the energy. By analogy to (3.8), the $m = 0$ ripplon contribution, E_0, to the energy is

$$E_0 = \pi L/6\hbar c_0 \beta^2 . \tag{3.36}$$

From (3.38), we see that the next most important contribution will come from the $m = 1$ phonons and ripplons combined. We write the frequency as

$$\omega^2 = \omega_1^2 + c_1^2 k^2 ,$$
$$\omega_1^2 = \frac{[g(a)/a][(R/a)^2 - 1]}{(R/a)^2 + 1} , \tag{3.37}$$
$$c_1^2 = [\sigma/\rho_0 g(a)]\omega_1^2 .$$

The $m = 1$ contribution to the energy is arrived at in the same fashion as was (3.5). Thus,

$$E_1 = (L/\pi)(1/\beta^2\hbar c_1)\sqrt{\tfrac{1}{2}}\pi(\hbar\beta\omega_1)^{3/2} e^{-\beta\hbar\omega_1} . \tag{3.38}$$

From the sum $E_0 + E_1$, the ratio of the specific heat to that of the bulk is computed to be

$$c/c_{\text{bulk}} = (5/2\pi^2)(s/c_0)(\hbar s\beta/R)^2 \times [1 + 6(\beta\hbar\omega_1/2\pi)^{3/2}(\tfrac{1}{2} + \beta\hbar\omega_1) e^{-\beta\hbar\omega_1}] . \tag{3.39}$$

Since $s/c_0 \sim 2 - 10$, we predict a considerable enhancement here over the full pore result given in (3.13). It is important to note that

$$\hbar\omega_1/k_B \sim [\hbar^2 g(a)/k_B^2 a]^{1/2} \sim 0.1 \text{ K}$$

(for films which are not too thin). Consequently, (3.39) is applicable only for temperatures rather smaller than 0.1 K.

If the instability of (3.24) is too closely approached, (3.36) is no longer applicable. As is seen from (3.25), ω must be replaced by

$$\omega = [(a/2\rho_0\sigma)[(R/a)^2 - 1]]^{1/2} k^2 \equiv \alpha k^2 . \tag{3.40}$$

This gives an energy[32]

$$E_{0c} = 2L \int_0^\infty \frac{dk}{2\pi} \frac{\hbar\alpha k^2}{e^{\beta\hbar\alpha k^2} - 1} = \frac{L}{2\pi} \frac{(k_B T)^{3/2}}{\sqrt{\hbar\alpha}} \Gamma(\tfrac{3}{2})\zeta(\tfrac{3}{2}) , \tag{3.41}$$

so that the leading term in (3.39) is replaced by

$$c_c/c_{\text{bulk}} = (45/8\pi^2)(\hbar^5 s^6 \beta^5/\alpha R^4)^{1/2}\Gamma(\tfrac{3}{2})\zeta(\tfrac{3}{2}) . \tag{3.42}$$

The low-temperature specific heat near the instability is thus enhanced over that in (3.39) by a factor $T^{-1/2}$. There is, however, no infinity in c/c_{bulk} as $c_0 \to 0$, as careless use of (3.39) might suggest.

At sufficiently low temperatures, the specific heat should show interesting behavior as a function of coverage. For low coverages, (3.39) should obtain. As coverage is increased toward critical, c should rise in accordance with (3.42), and as the instability is passed and the pores fill up, c should drop to the relatively low value given in (3.13). The data of Tait and Reppy[28] at $T = 0.1$ K have roughly this character, in that c is smaller for full pores than for partial coverage. However, as previously remarked, their data near $T = 0.1$ K still indicate large effects from the solid He^4 near the Vycor walls. Further, $T = 0.1$ K is really not sufficiently small for (3.39) and (3.42) to apply, and the rise near critical coverage might well be partly masked by the existence of a distribution of pore sizes in real Vycor.

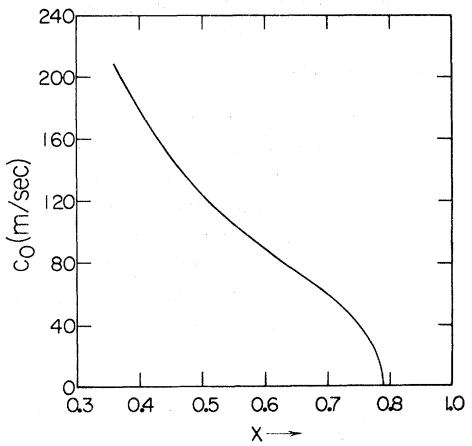

FIG. 1. Velocity c_0 of $m = 0$ ripplons vs the coverage variable $x = 1 - a^2/R^2$ for $R = R_0$.

At low temperatures the velocity c_0 given in (3.25b) is the third-sound velocity v_3 for the system. If we assume that the thickness of any solid layer near the substrate walls is small compared to the film thickness, we may easily compute c_0 from the potential discussed below. For the case $R = R_0 = 29.4$ Å, the result is depicted in Fig. 1 as a function of coverage $x \equiv 1 - a^2/R^2$. One sees that c_0 decreases monotonically toward zero as the instability is approached. In a nonideal system, such as Vycor, where one expects a distribution of average pore radii as well as a variation of radius within a given pore, the observed v_3 would reflect average flow characteristics.[30] In such a situation we would expect v_3 to decrease as the pores are filled, reaching a minimum when the average pore reaches the instability. Beyond that, as segments of pores are filled, the observed average velocity should rise since the velocity in the (microscopic) segments would be the faster fourth-sound velocity. Finally, when the pores are all filled, the waves will propagate at the (average) fourth-sound velocity. This qualitative behavior has been observed.[29]

Finally, we remark that at low T and away from the instability, ρ_n becomes

$$\rho_n = (k_B T)^2/3\hbar c_0^3 R^2 . \quad (3.43)$$

Since for appreciable pore filling (see Fig. 1), $c_0 \ll s$, the normal density in partially filled pores can be much larger than that for filled pores given by (3.16). This characteristic is borne out by recent measurements.[29] Quantitative agreement is lacking, however, a fact which we again attribute to deficiencies in our model when applied to Vycor. There is a clear need for experiments in more ideal substrates, such as Nuclepore filters, if there is to be definitive comparison between theory for a tractable model, such as the present one, and experimental data.

C. The instability and its associated metastable region

Earlier in this section [Eq. (3.24)] we discovered a long-wavelength dynamical instability associated with the $m = 0$ ripplons on the inner surface of a cylindrical shell of helium. This is clearly not specific to helium at low temperatures; since it follows from the equations of hydrodynamics, it will be true for any liquid, such as nitrogen, in a similar geometry.

We now examine the thermodynamics of the instability. Our derivation of (3.24) here will be more general than the previous one in that we don't restrict ourselves to $T = 0$. If P_l and P_V are, respectively, the equilibrium liquid and vapor pressures at the interface in the geometry of Fig. (4a), then, from (2.4),

$$P_V = P_l + \sigma/a . \quad (3.44)$$

Assuming the vapor to be ideal, and neglecting the small variation of $v_l \equiv m_4/\rho_0$ with pressure, we may integrate the Gibbs-Duhem relation $d\mu_0 = v\,dP$ at constant T to relate μ_0, for both liquid and vapor, to its value at the saturated vapor pressure P_0. Combining the results with (2.4), we easily obtain

$$\mu_V = \mu_0(P_0, T) + \beta^{-1}\ln(P_V/P_0) + U(a) , \quad (3.45a)$$

$$\mu_l = \mu_0(P_0, T) + v_l(P_l - P_0) + U(a) . \quad (3.45b)$$

Equating these two results and using (3.44) along with the simply demonstrated fact that $P_0 - P_V \ll \sigma/a$, we find $\ln(P_V/P_0) = -\beta v_l \sigma/a$. Consequently, (3.45a) gives

$$\mu = \mu_0(P_0, T) + U(a) - v_l\sigma/a , \quad (3.46)$$

for the chemical potential of the system. Next, we note that increasing the number N of particles in the system corresponds to decreasing the film radius a, and that a thermodynamic stability requirement for the system is $\partial\mu/\partial N \geq 0$.[33] Therefore, it follows from (3.46) and (2.13) that one must have $\sigma \geq \rho_0 a^2 g(a)$, if the film is to be stable. This is just the dynamical stability requirement of Eq. (3.24), confirming the association mentioned above between the long-wavelength mode stability and the film thermodynamic properties.

To understand in detail the meaning of the stability requirement we must discuss the potential $U(\vec{r})$. We preface this discussion by remarking that in the remainder of this section, R must be interpreted as the substrate pore radius, and not the effective film radius as above. From (2.21), one finds

$$U(a) = -(3\pi\alpha/2R^3)F(\tfrac{3}{2}, \tfrac{5}{2}; 1; y^2) , \quad (3.47)$$

where $y \equiv a/R$ and F is a hypergeometric function. Details of the calculation are given in Appendix A. $U(a)$ is a monotonically decreasing function of a which reduces to the expected planar result

$$U(a) \approx -\alpha/(R-a)^3 , \quad (3.48)$$

for $(R/a) - 1 \ll 1$, and, since $F(a, b; c; 0) = 1$, has the value $-3\pi\alpha/2R^3$ at $a = 0$. The function $(R^3/3\pi\alpha)U(a) + \frac{1}{2}$ is plotted in Fig. 2. We use the numerical value $\alpha = 1.6\times10^{-37}$ erg cm^3, from the results of Sabisky and Anderson,[21] for a planar film of helium on SiO_2 (Vycor is composed of approximately 99% SiO_2). It is clear from Fig. 2 that the instability limit, defined by the equality in (3.24), will be reached for a sufficiently thick film. We show below that the instability occurs because for a sufficiently thick film it becomes energetically

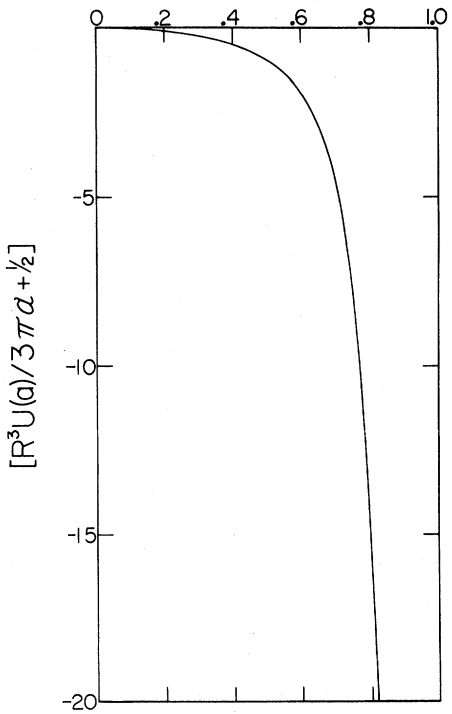

FIG. 2. Substrate potential $U(a)$ as a function of relative inner radius $y = a/R$ and the van der Waals coefficient α.

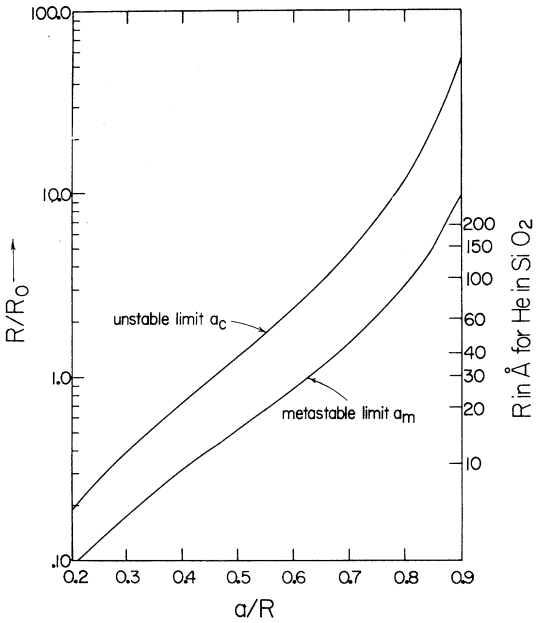

FIG. 3. Critical values of the inner radii a_m and a_c divided by pore radius R, expressed as universal functions of the dimensionless variable R/R_0. As an example, the scaling appropriate to liquid helium on an SiO_2 substrate, $R_0 = 29.4$ Å, is shown on the right ordinate. The film is stable if $a > a_m$, metastable if $a_c < a < a_m$, unstable if $a < a_c$.

favorable to fill the pore in order to reduce the surface energy (see Fig. 4).

The equation determining the limiting radius of stability, $a_c \equiv y_c R$ is easily found from (3.24), (3.47), and Eq. (A6) of Appendix A. In terms of the scaling parameter

$$R_0 = (3\pi\alpha/\sigma v_l)^{1/2} , \tag{3.49}$$

and the associated Legendre function $P^1_{3/2}$, this equation is

$$(R/R_0)^2 = y_c^2(1-y_c^2)^{-5/2} P^1_{3/2}[(1+y_c^2)/(1-y_c^2)] . \tag{3.50}$$

The universal curve generated by this equation is displayed in Fig. 3. As a specific illustration, one axis of this figure shows the scaling for He^4, in Vycor, for which $R_0 = 29.4$ Å.

There exists a regime of film thickness $a_c < a < a_m$, for which the symmetric configuration of Fig. 4(a) is metastable relative to the partially filled configuration sketched in Fig. 4(b), in that the latter is of lower free energy but is not accessible without a macroscopic deformation of the former. In a preliminary note on this work,[9] we determined a_m from an argument involving minimization of the free energy, but we did not determine the detailed shape of the interface in Fig. 4(b). Here we take an alternate tack which allows us to obtain both a_m and the interfacial shape.

If the pore is connected to a particle reservoir, rather than being closed (both approaches lead, of course, to the same result for a_m), minimization of the grand free energy leads to (2.9),[15] which, for present purposes, we write as

$$P_g(\vec{r}) = P_l(\vec{r}) + \sigma K(\vec{r}) . \tag{3.51}$$

Using arguments similar to those connecting (3.44)–(3.46) allows one to put (3.51) in the form[34]

$$k_B T \ln(P_\infty/P_0) = U(\vec{r}) - v_l \sigma K(\vec{r}) . \tag{3.52}$$

In order to use (3.52) to calculate the stable surface shape $Z(r)$, we note that cylindrical symmetry requires that the variables in (3.52) be functions only of $|\vec{r}| \equiv r$. Further, as (3.52) must hold everywhere on the surface, in particular in the asymptotic region where $r = a_m$ and $K(r) = 1/a_m$, (3.52) becomes

$$RK(r) = (R_0^2/R^2)[f(y_m) - f(y)] + 1/y_m , \tag{3.53}$$

where [see (3.47)].

$$f(y) = -(R^3/3\pi\alpha) U(r) , \tag{3.54}$$

and $y_m \equiv a_m/R$.

The next step is to relate $K(r)$ to the surface shape function $Z(r)$. This is done using the techniques of differential geometry,[35] which yield

$$RK(r) = \{z''(y) + z'(y)[z'^2(y)+1]/y\}[z'^2(y)+1]^{-3/2} , \tag{3.55}$$

where

$$z(y) \equiv Z(r)/R . \tag{3.56}$$

We search for a solution $z(y)$ to (3.53) and (3.55) which starts out with zero slope at $y = 0$ and which

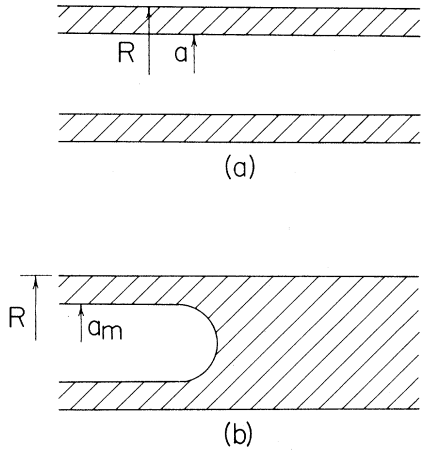

FIG. 4. Liquid (hatched area) adsorbed in cylindrical pores of radius R, viewed in longitudinal section. (a) Film adsorbed uniformly and symmetrically on walls. (b) Partially filled and partially empty pore geometry, occurring when the number of atoms present exceeds the critical number.

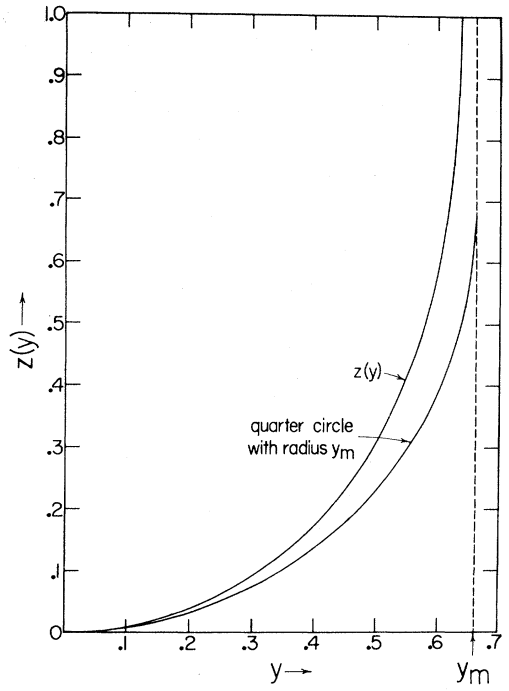

FIG. 5. Detailed stable surface shape for $R_0/R = 0.70$ and $y_m = a_m/R = 0.66$. A quarter circle, corresponding to a hemispherical end shape, is shown for comparison.

tends asymptotically to infinity at some $y = y_m$. Simply substituting the form $z(y) = \gamma y^2 + O(y^3)$ gives

$$z(y) = \tfrac{1}{4}[(R_0^2/R^2) f(y_m) + 1/y_m] y^2 + O(y^3) \ . \quad (3.57)$$

Using (3.57) to begin the numerical integration, we have obtained solutions for $z(y)$ and y_m as functions of R/R_0. For each value of R/R_0, there is only one value of y_m for which $z(y)$ behaves like (3.57) near $y = 0$, and tends asymptotically to infinity at $y = y_m$. The result for $R_0/R = 0.70$ and $y_m = 0.66$ is shown in Fig. 5. For purposes of comparison, the case of a hemispherical end surface, commonly assumed in previous work on the subject, [14] is also shown.

We can show that the y_m's found in this way are identical to those obtained in our earlier note. [36] If we multiply (3.53) by y, integrate from zero to y_m, use the relation

$$\frac{d}{dy}\{yz'(y)/[z'^2(y)+1]\}$$
$$= \{yz''(y) + z'(y)[z'^2(y)+1]\}[z'^2(y)+1]^{-3/2} \ ,$$

and note that $z'(0) = 0$ and $z'(y_m) = \infty$, we immediately arrive at our previous result

$$R^2/R_0^2 = y_m f(y_m) - \frac{2}{y_m}\int_0^{y_m} y f(y)\, dy \ . \quad (3.58)$$

A plot of y_m vs R/R_0 is shown in Fig. 3.

D. Sorption

In this subsection we apply our previous results to the calculation of sorption isotherms, i.e., curves of fractional pore filling versus the reduced pressure $p \equiv P/P_0$, where P is the pressure external to the pore. We assume that on filling, the metastable configuration is followed up to $r = a_c$, whereas on emptying, the stable configuration occurs. This explanation of hysteresis, which has in fact been observed in numerous experiments involving porous media and a variety of adsorbates (see Ref. 34), is new. Note that the critical film thickness $(R - a_c)$ is actually an upper limit for the metastable regime. The sophisticated treatment required to derive a more accurate result is not justified, however, since any real system has constrictions which would nucleate the transition between configurations (4a) and (4b). We discuss below the results obtained for the case of a material possessing a distribution of pore radii, which is useful for understanding the behavior of a real nonuniform system. First, however, we treat the case of a material having a unique pore size.

1. Single pore radius

Assuming that all the pores in Vycor are independent and have the same radius R, the filling fraction x, for the configuration in Fig. 4(a) is

$$x = (R^2 - r^2)/R^2 = 1 - y^2 \ . \quad (3.59)$$

Here, as above, $r = Ry$ is the inner radius of the film. As a function of p, x is determined by (3.52) with $K = \sigma/r$, and U is obtained from (3.47). In terms of R_0, $R_T \equiv \beta\sigma v_l$, and $f(y)$, (3.52) takes the form

$$p = \exp\{-(R_T/R_0)(R_0^3/R^3)[f(y) + R^2/R_0^2 y]\} \ . \quad (3.60)$$

The relation between p and x is obtained numerically from (3.59) and (3.60). Some general features of the curve $x(p, R)$ are easily discerned. As $x \to 0$ (i.e., $y \to 1$), $p \to 0$ since the potential $\sim -f(y)$ approaches minus infinity near the pore walls. p rises as x is increased (y decreased). When the instability is approached, the argument of the exponential in (3.60) goes through a maximum. Hence, $x(p, R)$ has an infinite derivative at the pressure p_c of the maximum. The pores will simply fill up, i.e., x will increase vertically toward one, when p_c is reached—since p_c is larger than the constant pressure corresponding to the stable configuration of Fig. 4(b), as will be seen momentarily. (This constant value of $p = p_c$ for a variable number of particles is analogous to that obtaining for liquid-vapor equilibrium; the completely and partially filled regions of the pore cor-

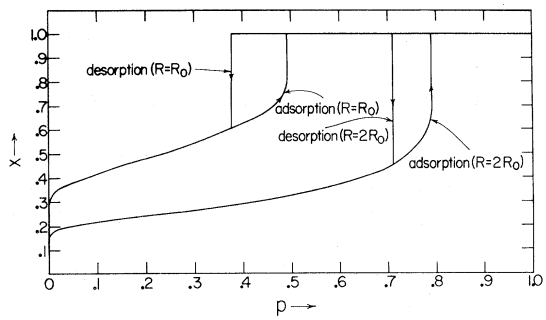

FIG. 6. Sorption isotherms for helium in pores of radii $R = R_0$ and $R = 2R_0$.

respond to the two coexisting phases.) When x is very near unity, it must turn sharply and proceed almost horizontally to very near the point $x = 1$, $p = 1$. This occurs for two reasons. First, the pressure needed to build up even a thin planar film on the outside of the Vycor is large. For example, for a film thickness $d = 40$ Å, and $T = 1$ K, $p = \exp(-\beta\alpha/d^3) = 0.982$. Secondly, the number of atoms involved in filling up the ends of the pores and in depositing the planar film is quite small compared to the number of atoms needed to fill the pores (~ 30% of the Vycor volume is taken up by pores).

The pressure p_m corresponding to the stable configuration is found from (3.60) with $y = y_m$. Since $y_m < y_c$ and since $f(y) + R^2/R_0^2 y$ decreases monotonically from infinity at $y = 1$ to its minimum at $y = y_c$, it is clear that $p_m < p_c$. Further, as p_m is (except for end effects) independent of the position of the curved interface, pores in this configuration are filled or emptied at constant pressure. On emptying, then, p must be reduced to p_m before anything happens. At p_m, the pores empty as the curved surface moves down. Finally, when only cylindrical helium shells are left with inner radii a_m, further desorption is governed by (3.60).

The curves for adsorption and desorption are plotted in Fig. 6 for the case $T = 2.02$ K corresponding to the results of Brewer and Champeney.[25] The two cases $R = R_0$ and $R = 2R_0$ are shown to provide some feeling for the dependence on R. Increasing T has roughly the same qualitative effect as increasing R.

2. *A distribution of pore radii*

It is clear from Fig. 6 that a distribution of pore sizes would smear out the rather abrupt character of the curves. Such smearing is observed experimentally.

To include the effect of a distribution, we define $x_+(p, R)$ as the filling fraction for the adsorption branch in a pore of radius R at reduced pressure p. Then,

$$x_+(p, R) = \Theta(p - p_c(R))\,\nu(R) + \Theta(p_c(R) - p)\,x(p, R)\,\nu(R)\ , \tag{3.61}$$

where $\Theta(x) = \{1 \text{ for } x > 0,\ 0 \text{ for } x < 0\}$ is the unit step function, $x(p, R)$ is the filling fraction used above, $p_c(R)$ is the relative pressure at the instability for given R, and $\nu(R)$ is the number of particles in a filled pore having radius R. Then, if $s(R)$ is the distribution function for pore sizes, the filling fraction for all pores is

$$x_+(p) = \int_0^\infty dR\, s(R)\, x_+(p, R)\ . \tag{3.62}$$

Using (3.61), this becomes

$$x_+(p) = \int_0^{R_c(p)} dR\, s(R)\,\nu(R) + \int_{R_c(p)}^\infty dR\, s(R)\, x(p, R)\,\nu(R)\ . \tag{3.63}$$

Here, the critical radius $R_c(p)$ is the solution of

$$p_c(R_c(p)) = p\ . \tag{3.64}$$

$R_c(p)$ is a monotonically increasing function of p which approaches infinity as $p \to \infty$. It is obtained from (3.60) and plotted in Fig. 7 for $T = 2.02$ K. We take $\nu(R) = \pi L R^2$, where L should be thought of as an average pore length. Using the normalization condition

$$1 = \int_0^\infty dR\, \pi L R^2 s(R)\ , \tag{3.65}$$

(3.63) becomes simply

$$x_+(p) = \frac{\int_0^{R_c(p)} dR\, R^2 s(R) + \int_{R_c(p)}^\infty dR\, R^2 s(R)\, x(p, R)}{\int_0^\infty dR\, R^2 s(R)} \tag{3.66}$$

This result holds on continuous filling from $x = 0$ to $x = 1$. For continuous desportion, we use

$$x_-(p) = \frac{\int_0^{R_m(p)} dR\, R^2 s(R) + \int_{R_m(p)}^\infty dR\, R^2 s(R)\, x(p, R)}{\int_0^\infty dR\, R^2 s(r)}\ , \tag{3.67}$$

where $R_m(p) > R_c(p)$ is defined by

$$p_m(R_m(p)) = p\ , \tag{3.68}$$

and plotted in Fig. 7. $R_m(p)$ appears because of our assumption that a pore of radius R, on the desorption branch, does not begin to empty until the pressure reaches $p_m(R)$.

Since there is no detailed information available for $s(R)$ in Vycor, we have carried out some calculations assuming a Gaussian distribution:

$$s(R) = \exp\{-\tfrac{1}{2}[(R - R_A)/\Delta]^2\}\ , \tag{3.69}$$

where R_A is the average pore radius and Δ the standard deviation. Both the adsorption curve $x_+(p)$ and the desorption curve $x_-(p)$ are plotted in Fig. 8 for $T = 2.02$ K, $R_A = R_0 = 29.4$ Å, and $\Delta = 0.2$

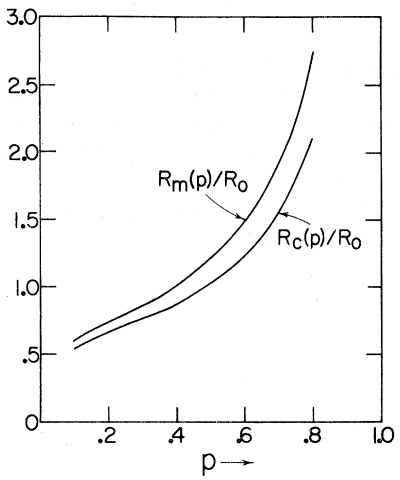

FIG. 7. Metastable and critical radii, $R_m(p)$ and $R_c(p)$, as functions of the reduced pressure $p \equiv P/P_0$.

$\times R_0 = 5.88$ Å. This data of Brewer and Champeney[25] for $T = 2.02$ K are also plotted. We have not attempted a detailed fit of the data using R_A and Δ as parameters, but the curves shown in Fig. 8 represent about the best that can be achieved with the distribution (3.69). Changes in either R_A or Δ tend merely to move the curves up or down without changing the size of the hysteresis loop. An asymmetric distribution minimizing the effect of smaller pore sizes would help matters.

To this point we have only discussed the cases of continuous adsorption and desorption. It is of interest to ask what happens if the pores are continuously filled up to some point $x < 1$ and then the pressure is decreased. If p_d is the maximum pressure reached, then the filling fraction will be given by

$$x_d(p) = \frac{\int_{R_c(p_d)}^{\infty} dR\, R^2 s(R) + \int_{R_c(p_d)}^{\infty} dR\, R^2 s(R) x(p,R)}{\int_0^{\infty} dR\, R^2 s(R)}\,, \tag{3.70}$$

until $x_d(p)$ reaches the desorption curve $x_-(p)$, at which point this latter curve will be followed. The reason for this is that the pressure in those pores just becoming critical at p_d must be reduced to that value for which these pores would begin to empty on desorption before regular desorption occurs for all pores. The point of intersection with the desorption curve is then $x_-(p_m(R_c(p_d)))$. This situation is depicted in Fig. 8 for the case $p_d = 0.50$.

Measurements of this type for varying p_d can in principle be used to determine the distribution $s(R)$, given that the rest of the theory is correct. In fact, from (3.66) and (3.70) one finds

$$\left.\frac{d}{dp}\left[x_+(p) - x_d(p)\right]\right|_{p=p_d} = R^2 s(R) \frac{dR_c(p)}{dp}\left[1 - x(p,R)\right] \Big/ \left.\int_0^{\infty} dR' R'^2 s(R')\right|_{\substack{p=p_d \\ R=R_c(p_d)}} \tag{3.71}$$

Unfortunately, the requisite measurements have not yet been carried out.

E. Possible He^3 surface superfluidity in cylindrical pores

It is well known[37] that there is a bound state for a He^3 atom on a planar free surface of bulk superfluid He^4, and that this makes possible the existence of a two-dimensional Fermi liquid on the free surface. The density, and hence degeneracy temperature, of this liquid can be varied over a wide range. The experiments of Eckardt *et al.*[37] indicate that the effective interaction between the surface He^3 quasiparticles is quite weak (the sign is undetermined).

By analogy to the theory of Bardeen, Baym, and Pines[38] for He^3-He^3 quasiparticles in bulk mixtures of He^3 in superfluid He^4, we can view the interaction between surface He^3 quasiparticles as the sum of a repulsive, fairly short range, direct interaction and an attractive, longer-range interaction due to exchange of single He^4 excitations. The results of Eckardt *et al.*[37] suggest that these two effects approximately cancel for planar surfaces. If, however, the He^3's are adsorbed on the inner surface of a He^4 film in a cylindrical pore, the situation may be quite different. The He^4 excitations are, as we have seen, drastically altered. In particular, in the region of the instability [Eq. (3.24)] the $m = 0$ ripplons become very soft. We

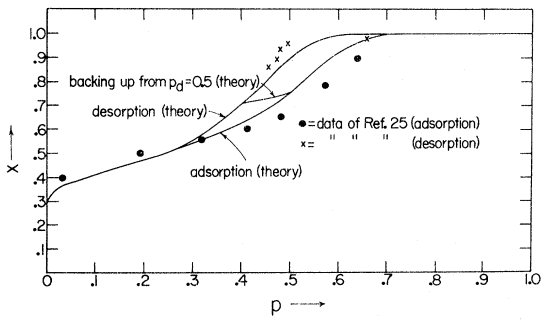

FIG. 8. Pore radius averaged theoretical sorption isotherms (solid lines) as compared with experimental data of Ref. 25 for $T = 2.02$ K. The mean radius is $R_A = R_0 = 29.4$ Å, and the distribution width $\Delta = 0.2R_0 = 5.88$ Å.

suggest that this softening, which will enhance the attractive part of the interaction due to single excitation exchange might be sufficient to cause superfluidity in the He^3 surface Fermi liquid.[39]

One way to observe the superfluidity suggested here might be to look for rapid He^3 concentration equilibration between two different gaseous mixtures of He^3 and He^4 connected by a rod of porous Vycor or a Nuclepore filter. Other possibilities might be to use NMR techniques (which have been a primary diagnostic tool in the study of superfluid He^3) or the third-sound resonance technique of Ref. 29 (which will show a He^3 contribution only if the He^3 is superfluid).

IV. PLANAR FILMS

A. Spectrum

Consider a film of thickness D on a substrate which occupies the half space $z<0$. Then the surface curvature operator of Eq. (2.10) satisfies

$$K_1^{op}\zeta(\vec{r}_s,t)=\left(\frac{\partial^2}{\partial x^2}+\frac{\partial^2}{\partial y^2}\right)\zeta(\vec{r}_s,t)\ . \tag{4.1}$$

Letting

$$\varphi(\vec{r})=e^{i\vec{q}\cdot\vec{r}}\,\varphi_q(z)\ , \tag{4.2}$$

where $\vec{q}$ is a vector in the x-y plane, Eqs. (2.14) and (2.15) yield

$$\left[\frac{d^2}{dz^2}+\left(\frac{\omega^2}{s^2}-q^2\right)\right]\varphi_q(z)=0\ , \tag{4.3}$$

$$\left(g(\zeta+D)+\frac{\sigma}{\rho_0}\,q^2\right)\frac{d\varphi_q}{dz}\bigg|_{z=\zeta+D}=\omega^2\,\varphi_q(\zeta+D)\ . \tag{4.4}$$

There are two possible forms for φ_q. The first, called a ripplon because of its localization near the surface, satisfies $q^2-\omega^2/s^2\equiv l^2>0$:

$$\varphi_q(z)=\varphi_q^0(e^{lz}+e^{-lz})\ , \tag{4.5}$$

where we have used the boundary condition $\varphi_q'(z)=0$ at the substrate. From this equation and the interfacial condition (4.4), evaluated for small amplitude fluctuation ζ, we obtain the ripplon eigenvalue equation

$$\omega^2(q)=l[g(D)+\sigma q^2/\rho_0]\tanh(lD)\ , \tag{4.6a}$$

$$q^2-\omega^2/s^2=l^2>0\ . \tag{4.6b}$$

It is easy to see that there exists a unique l value which simultaneously solves these equations for any fixed q. For $lD\ll 1$, Eq. (4.6) yields the relation

$$\frac{q^2}{l^2}=\frac{1+gD/s^2}{1-\sigma Dl^2/\rho_0 s^2}\ .$$

For films thicker than about 10 Å, $gD\ll 1$, in which case $q\to l$ in the long-wavelength limit. Thus for $qD\ll 1$, we find from (4.6):

$$\omega=cq\ ,\quad qD\ll 1, \tag{4.7}$$

$$c^2=g(D)D\ . \tag{4.8}$$

These acoustic modes are called third sound in He^4 films.[5,7,8] In the opposite limit, $lD\gg 1$,

$$\frac{q^2}{l^2}=\frac{1+g/s^2l}{1-l/l_0}\approx\frac{l^2}{1-l/l_0}\ . \tag{4.9}$$

Here we have defined $l_0=\rho_0 s^2/\sigma\approx 2.3$ Å^{-1} and used the fact that $g/s^2l\ll gD/s^2\ll 1$ in this regime, for films thicker that about 10 Å. As discussed in Sec. II, we are using a hydrodynamic description and cannot trust our results for large wave vector. Thus we are concerned only with $l<l_0$, and for this case again find $l\approx q$. Then Eq. (4.6a) yields

$$\omega^2(q)\approx q[g(D)+\sigma q^2/\rho_0]\ . \tag{4.10}$$

In practice, neither of the approximations (4.9) and (4.10) suffices for the temperature and thickness regimes of interest. We display in Fig. 9 the calculated values of $\omega(q)$ for the ripplons necessary for determining low-temperature phenomena. For large D the curves coalesce for $q\gtrsim 0.04$ Å^{-1} to the bulk incompressible capillary wave limit of Eq. (4.10), $\omega^2=\sigma q^3/\rho_0$.

Note that the ripplon spectrum in planar geometry possesses no instability comparable to that found

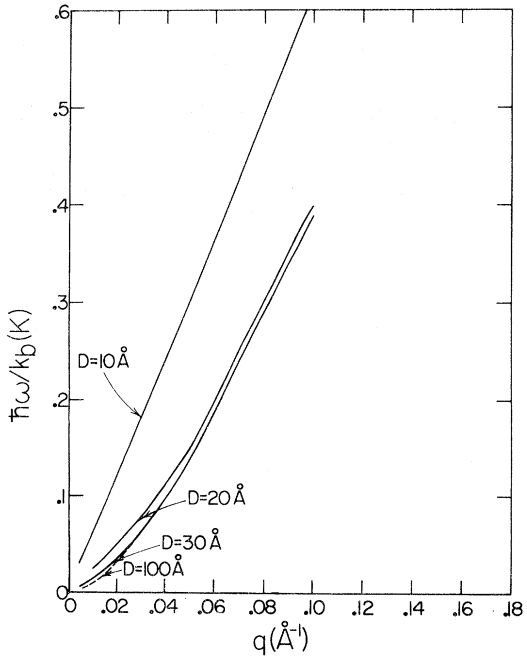

FIG. 9. Ripplon frequency as a function of wave vector for planar films of thickness D. The spectrum has been calculated for the case of helium on quartz, for which $\alpha=1.6\times10^{-37}$ erg cm^3.

in cylindrical geometry. One might anticipate such an instability because a very thick film is thermodynamically unstable relative to a nearly hemispherical film which has a smaller surface area. However, no instability occurs because the planar configuration is stable with respect to small oscillations (those considered in the dynamics) and the thermodynamic instability in global, involving macroscopic deformation. An interesting aspect of the problem is that this global instability is manifested in a divergence of the total mean-square surface fluctuation, obtained by summing over all modes. This instability is removed, however, when the gravitational field is taken into account.[40]

We can now proceed to discuss the case $\omega^2/s^2 - q^2 \equiv k^2 > 0$. The solution of Eqs. (4.3) and (4.4) with a vanishing vertical velocity at the substrate is an oscillatory mode which we identify as a phonon, since it extends throughout the film:

$$\varphi_q(z) = \varphi_q^0 \cos kz \ , \tag{4.11}$$

$$\omega^2(q, k) = -k\,[g(D) + \sigma q^2/\rho_0] \tan kD \ , \tag{4.12}$$

$$\omega^2/s^2 - q^2 = k^2 > 0 \ . \tag{4.13}$$

In contrast to the ripplon case, there exists here an infinite number of k values which satisfy Eqs. (4.12) and (4.13) for any given q. From the properties of the tangent functions one finds that a solution k_n exists, $\frac{1}{2}n\pi < k_n D < \frac{1}{2}(n+1)\pi$, for each odd integer n. For $n \gg 1$, the relation becomes $k_n = n\pi/2D$. In terms of the wavelength $\lambda = 2\pi/k$,

$$D \cong \tfrac{1}{4} n\lambda, \quad \text{odd } n \gg 1 \ . \tag{4.14}$$

This corresponds to the free surface being an antinode of oscillation, the result one would expect for a normal mode in the absence of our surface boundary condition.

There is special interest in the phonon modes because Sabisky and Anderson[20,21] and Blackford[41] have explored them by measuring the loss of monochromatic phonons incident on a helium film from the substrate. Resonances were observed when Eq. (4.14) was satisfied to a rather good approximation.[42] We next calculate the correction to this equation for small n.

The matching equations at the solid-film boundary are

$$s^2\,[k_n^2(q) + q^2] = s_s^2 q_s^2 \ , \tag{4.15}$$

$$q_s \sin\theta_s = q \ , \tag{4.16}$$

where s_s and θ_s are the speed and incident angle of the phonons from the solid. Since $s_s \gg s$, we find

$$k_n \sin\theta_s \approx s_s q/s \tag{4.17}$$

By examining the q dependence of k_n, it is possible to show that for these experiments [$q_s \approx (10^5 - 10^6)$ cm^{-1}], it is sufficient to determine k_n at $q = 0$. We obtain from (4.12) and (4.13) the wave vector at the nth resonance,

$$k_n(0) = (n\pi/2D)(1 + 4gD/n^2 s^2 \pi^2) \ , \tag{4.18}$$

to lowest order in the second term in brackets. This term is about 0.05 for $D = 10$ Å, $n = 1$, and decreases rapidly with increasing D and n. Thus one would expect significant deviation from the relation (4.14) only for very thin films. The available data do not extend into this regime.

B. Thermodynamic properties

Calculations can be performed for several regimes of interest. For low temperature, we use the numerical calculations of the ripplon spectrum and the analytic expression for the phonons. For intermediate temperature, $0.5 < T < 1.2$ (K), our approximations for the spectrum are invalid, so no reliable prediction is possible. For higher temperature, $1.2 < T < 2$, we can determine the films's properties from an approximate form of the spectrum at large q obtained via microscopic theory of surface excitations. Finally, we are able to derive analytic expressions in the thick-film limit. In the present context, the measure of thickness with which we compare is the phonon thermal wavelength,

$$\lambda = \beta \hbar s \ . \tag{4.19}$$

1. Low temperature

We consider first the low temperature regime, $\lambda \gg D$. From Eq. (4.13), the lowest phonon energy is $\hbar\omega_1 = \hbar s k_1(0) \gtrsim \hbar s \pi/2D$, corresponding to $q = 0$, so the phonon contributions to the thermal properties is exponentially small at low temperature. Because of this, the phonon contribution is negligible relative to the ripplon contribution, which we shall see has a power law dependence on T. Let the frequency corresponding to the nth value of k_n be $\omega_n^2 = s^2(k_n^2 + f_n q^2)$, where $k_n \equiv k_n(0)$, and n is an odd integer. The energy is from Eq. (2.17):

$$E_p = \sum_{q,n} \hbar s (k_n^2 + f_n q^2)^{1/2} (e^{\beta\hbar\omega_n(q)} - 1)^{-1} \ .$$

Converting the sum over q to an integral, the upper limit of which we may take at low T to be infinity,

$$E_p = \frac{\hbar s A}{2\pi\lambda^3} \sum_n f_n^{-1} \int_{x_n}^{\infty} dx\, x^2 (e^x - 1)^{-1} \ , \tag{4.20}$$

$$x_n = k_n \lambda \ . \tag{4.21}$$

Since $x_n \approx \pi\lambda n/2D \approx 29\, n$ Å$/DT \gg 1$ at low T, only the $n = 1$ term of the sum contributes, yielding

$$E_p \cong (A/2\pi f_1 \beta) k_1^2 e^{-x_1} (1 + 2/x_1 + 2/x_1^2) \ . \tag{4.22}$$

The specific heat (per unit volume) is, neglecting terms of order x_1^{-2} and letting $k_1 \cong \pi/2D$,

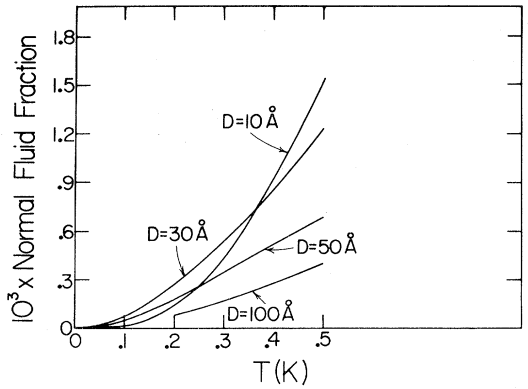

FIG. 10. Normal fluid fraction $10^3\rho_n/\rho$ in the ripplon-dominated low temperature regime for planar films of thickness D.

$$c_s \cong (\hbar s\pi^2/16D^4T)e^{-x_1}(1+3/x_1)\ . \tag{4.23}$$

Finally, the normal-fluid density is from Eq. (2.18), after integrating over q,

$$\rho_n = (\hbar^2\beta/4\pi D\lambda^4)\sum_i f_i^{-2}\int_{x_i}^{\infty} dx\, x(x^2-x_i^2)e^x(x^x-1)^{-2}\ . \tag{4.24a}$$

$$\rho_n = (\hbar^2\beta/4\pi D\lambda^4)\sum_i f_i^{-2}\int_{x_i}^{\infty} dx\,(3x^2-x_i^2)(e^x-1)^{-1}\ . \tag{4.24b}$$

At low T, the $i=1$ term dominates the sum, so to lowest order,

$$\rho_n = (x_1^2e^{-x_1}/2\pi D\,\beta^3\hbar^2s^4)(1+3/x_1+3/x_1^2)\ , \tag{4.25}$$

$$\rho_n \approx (\pi e^{-x_1}/8s^2\beta D^3)(1+3/x_1+3/x_1^2)\ , \tag{4.26}$$

where in the last expression we let $k_1 \approx \pi/2D$.

We turn to the ripplon contribution, which dominates the low-T thermal behavior. At very low temperature the characteristic wave vector satisfies $qD \ll 1$ and the acoustic limit Eq. (4.7) obtains. The criterion is $T \ll \hbar c/Dk_B$, which is about 0.1 K for $D = 20$ Å or 0.01 K for $D = 50$ Å. Then using Eqs. (2.17) and (4.7), the energy is

$$E = \zeta(3)A/\pi\beta^3\hbar^2c^2\ , \tag{4.27}$$

where $\zeta(x)$ is the Riemann ζ function, and we have let the upper limit of the q integral be infinity. The specific heat is then

$$c_s = 3\zeta(3)\,k_B^3\,T^2/\pi Dc^2\hbar^2\ . \tag{4.28}$$

By Eq. (4.8), $c^{-2} \propto D^3$, so the specific heat varies as D^2, owing to the softening of the modes with increasing D. The quadratic dependence on T corresponds to the two-dimensional character of the modes. Comparing with the bulk specific heat, which is determined at low T by the phonon contribution, we find (for a quartz substrate)

$$c_{s\ \mathrm{film}}/c_{s\ \mathrm{bulk}} \cong 1.67\ \nu^2/T\ , \tag{4.29}$$

where $\nu = Dn^{1/3} \approx D/3.6$ Å is the number of "layers" in the film, and n is the bulk density. Thus the film specific heat is greatly enhanced over the bulk result. Finally, the normal-fluid density is

$$\rho_n = 3\zeta(3)/2\pi D\beta^3\hbar^2c^4\ , \tag{4.30}$$

which varies as D^5T^3.

As indicated above, these results are valid only at very low T. As seen in Fig. 9, the spectrum deviates from $\omega = cq$ at wave vectors corresponding to a rather low temperature. Over a limited regime of higher temperature we can trust the calculated spectrum (4.6) and numerically integrate to find the thermal properties, which remain ripplon dominated. The results for the normal-fluid density and specific heat of a helium film on quartz are shown in Figs. 10 and 11. Figure 11 also shows the bulk specific heat, which is significantly smaller. The bulk normal-fluid fraction is negligible in the scale of Fig. 10. For $T \gtrsim 0.3$ K, the important regions of the ripplon spectrum are essentially independent of D. Thus both c_s and ρ_n vary inversely with D (see part 3 of this section). In the very low temperature regime we revert to the completely different behavior predicted by Eqs. (4.28) and (4.30). Thus there is a reversal of the relative ordering of thick and thin films, although this occurs at too low a temperature to be evident in the specific-heat prediction of Fig. 11.

No presently available data[43] are adequate to test

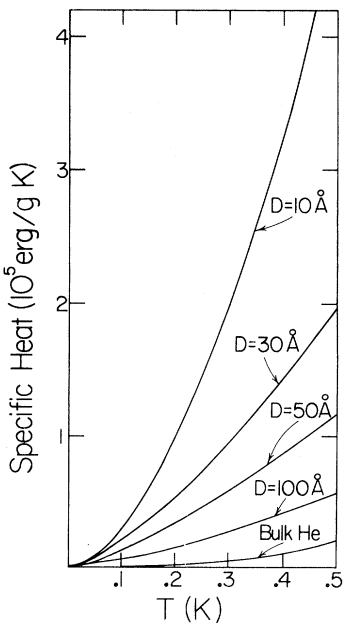

FIG. 11. Specific heat (per gram) at low temperature for planar films. Also shown for comparison is the bulk specific heat.

the predictions of this section. Clearly, experiments probing this regime would be of great value.

2. High temperature ($T \gtrsim 1.2$ K)

The thermal properties of bulk liquid helium at high temperature are determined by the roton region of the spectrum, for which the energy is given by $\hbar\omega = \Delta + \hbar^2(q-q_0)^2/2\mu$. It is reasonable to investigate the possible existence of an analogous minimum in the spectrum of surface excitations at large wave vector.[44] Two pieces of evidence have a bearing on this problem. Edwards, Eckardt, and Gasparini[45] have calculated the ripplon spectrum of the bulk liquid surface using a Hartree-like theory. The large q spectrum depends sensitively on a parameter characterizing the diffuseness of the liquid-vapor interface. Reasonable agreement with the measured surface tension can be obtained with a variety of spectra, some of which do possess a roton-like minimum.[46] If we assume such a surface roton exists, it may be parametrized by a form

$$\hbar\omega_{sr} = \Delta_s + \hbar^2(q-q_{s0})^2/2\mu_s \,. \tag{4.31}$$

We have fit several recent spectra[45,47] with $\Delta_s \approx 6.7$ K, $q_{s0} \approx 1.92$ Å^{-1}, $\mu_s \approx 0.12\, m_4$ and $\Delta_s \approx 8.5$ K, $q_{s0} \approx 1.93$ Å^{-1}, $\mu_s \approx 0.058\, m_4$, respectively.

Padmore[48] has applied the Feynman-Cohen[49] theory of three-dimensional helium to the two-dimensional system. Although such excitations may well be rather different from surface rotons in a film, it is of interest to explore the comparison. We fit his calculations for density $n^{2/3}$ with $\Delta_s \approx 9.25$ K, $q_{s0} \approx 1.74$ Å^{-1}, and $\mu_s \approx 0.25\, m_4$. However, it should be noted that similar calculations with Chester[50] for three-dimensional helium yield Δ about 2 K higher than experiment and q_0 about 0.2 Å^{-1} lower. In view of both this and the results of Edwards *et al.*,[45,47] it might be plausible to assume the bulk roton parameters, $\mu = 0.16\, m_4$ and $q_0 = 1.92$ Å^{-1}, for the surface roton. Assuming $\exp\delta \gg 1$, where $\delta = \beta\Delta_s$, the heat capacity and normal-fluid density are

$$C/A \cong (q_0/\hbar)\,\delta^2 e^{-\delta}(k_B^3\,\mu\,T/2\pi)^{1/2}[1+\delta^{-1}+3\delta^{-2}] \,, \tag{4.32}$$

$$\rho_n \cong (\hbar q_0^3/D)(\beta\mu/8\pi)^{1/2} e^{-\delta} \,. \tag{4.33}$$

Figure 12 is derived from the heat-capacity data of Bretz.[51] The important feature to note is that the thick-film ($\nu \gtrsim 9$) behavior is approximately that of an equivalent amount of bulk fluid. The thin-film heat capacity, however, tends asymptotically to roughly a constant, independent of D. This is reasonable evidence for negligible contribution of the bulk rotons at small D and a residual surface excitation contribution which does not depend significantly on D.

Calculations using Eq. (4.32) for the surface-roton heat capacity show that $\Delta_s \approx 2.5$ K is required to explain the small-D asymptotic data of Fig. 12. For such a small value, the approximation $\exp\delta \gg 1$ becomes invalid. Furthermore, we would expect that regions of the spectrum far from q_0 would contribute, and we do not know the details of $\omega(q)$. We can conclude only that large-q surface excitations probably explain the data, but these require a more careful treatment than presently exists.

3. Very thick films

The parameter λ/D was taken to be much greater than one in Sec. IV B 1, which permitted us to consider only the lowest wave vector of perpendicular motion, $k_1 \approx \pi/2D$, in phonon calculations. For the case of very thick films, the opposite limit $\lambda/D \ll 1$ will obtain, even for relatively low temperature. In this case, sums over perpendicular modes k_n in Eqs. (4.20) and (4.24) will be well approximated by an integral over a continuous variable k, as is conventionally performed for infinite systems. Corrections to this integral are of the form λ/D raised to some power, and represent the change in the particular function being computed on reducing D from infinity to a finite value.

Let us consider the sum in Eq. (4.20) for the phonon contribution to the energy

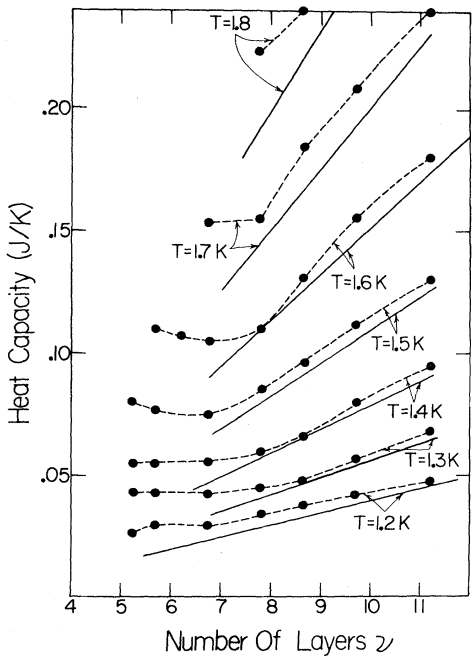

FIG. 12. Circles are heat capacity (with first layer subtracted) of He on graphite taken from data of Bretz (Ref. 51) with dashed lines drawn to aid the eye. Solid lines represent the heat capacity of an equivalent quantity of bulk liquid helium, assuming the first two layers do not contribute.

$$S \equiv \sum_{\text{odd } n} \int_{x_n}^{\infty} dx\, x^2 (e^x - 1)^{-1}\,, \quad x_n = \pi n \lambda / 2D\,, \tag{4.34}$$

in which we assume $f_n = 1$. This is incorrect by a few per cent for $n = 1$ and $D = 10$ Å, and much less for $n > 1$ and thicker films. In Appendix B, we show that

$$\sum_{\text{odd } n} g(x_n) = (\Delta x)^{-1} \int_0^{\infty} dx\, g(x) + \sum_{\text{odd } i} a_i (\Delta x)^i g_0^{(i)}\,. \tag{4.35}$$

Here, $\Delta x = x_n - x_{n-2} = \pi\lambda/D$, the first three coefficients a_i are calculated in Appendix B, and

$$g_0^{(i)} \equiv \left. \frac{d^i g}{dx^i} \right|_{x=0}\,. \tag{4.36}$$

The first term on the right side of Eq. (4.35) is the bulk value, and the sum is the desired correction, of which we determine the first finite term.

For the sum given in Eq. (4.34), the function g is the integral. In this case $g_0' = 0$ and $g_0^{(3)} = 1$. Thus from Eq. (4.25),

$$S \cong \frac{D}{\pi\lambda} \int_0^{\infty} dx \int_x^{\infty} dy\, y^2 (e^y - 1)^{-1} - \tfrac{7}{5760} (\pi\lambda/D)^3\,, \tag{4.37}$$

using the coefficient a_3 calculated in Appendix B. The integral gives $\frac{1}{15}\pi^4$, so that, from Eq. (4.20), the thick-film phonon energy is

$$E = (\hbar s \pi^2 \Omega / 30 \lambda^4)\left[1 - \tfrac{7}{384} (\lambda/D)^4\right], \tag{4.38}$$

where $\Omega = AD$ is the volume occupied by the film. The correction to the bulk is seen to be very small, even if T is low and the film relatively thin. For example, if $T = 0.5$ K and $D = 40$ Å, the correction is less than 2%.

We turn to the phonon contribution to ρ_n. In this case the integral in Eq. (4.24) becomes

$$g(x) = 3 \int_x^{\infty} dy\, y^2 (e^y - 1)^{-1} - x^2 \int_x^{\infty} dy\, (e^y - 1)^{-1}\,. \tag{4.39}$$

The first derivative of g vanishes at $x = 0$, but the third derivative diverges as $2/x$. We conclude that the film correction term, relative to bulk, is of order higher than $(\lambda/D)^2$ and lower than $(\lambda/D)^4$, but are unable to establish its value.

Let us now consider the bulk roton contribution. Taking $l^2 = k_i^2 + q^2$ and $\hbar\omega(l) = \Delta + \alpha(l - q_0)^2$, where $\alpha \equiv \hbar^2/2\mu$, we have from Eq. (2.18)

$$\rho_n = (\beta\hbar^2/4\pi D) e^{-\beta\Delta} \times \sum_{\text{odd } i} \int_{k_i}^{\infty} dl\, (l^3 - k_i^2 l) \exp[-\beta\alpha(l - q_0)^2]\,, \tag{4.40}$$

where we use $e^{\beta\Delta} \gg 1$. In this case the integral for g satisfies $g_0^{(1)} = 0 = g_0^{(3)}$, and $g_0^{(5)} = 32\alpha\beta q_0 \exp(-\alpha\beta q_0^2)$, where the derivatives of g are with respect to l. Using Eq. (4.35), we obtain for the sum in Eq. (4.40)

$$\frac{D}{\pi} \int_0^{\infty} dk \int_k^{\infty} dl\, (l^3 - k^2 l) \exp[-\beta\alpha(l - q_0)^2] + a_5 (\pi/D)^5 32\alpha\beta q_0\,.$$

With negligible error we extend the lower limit of the k integral to $-\infty$, which yields $\frac{1}{3} 2 q_0^4 (\pi/\alpha\beta)^{1/2}$, and substituting the value of a_5 from Appendix B we find

$$\rho_n = \hbar q_0^4 (\beta\mu/18\pi^3)^{1/2} e^{-\beta\Delta} \{1 + (D_r/D)^6 T^{-3/2} \times \exp(-T_r/T)\}\,, \tag{4.41}$$

$$D_r = \{31(\pi^{11}/2k_B^3\mu^3)^{1/2}\hbar^3 q_0^{-3}/40\,320\}^{1/6} \approx 1.8 \text{ Å}\,, \tag{4.42}$$

$$T_r = \hbar^2 q_0^2 / 2\mu k_B \approx 160 \text{ K}\,. \tag{4.43}$$

This length D_r is so small and T_r so large that the correction term in Eq. (4.41) is negligible. We conclude that the roton contribution to ρ_n is the same for the film as for the bulk fluid. The same result is found for the specific heat. In both cases this behavior follows from the high characteristic temperature T_r and wave vector q_0.

We observed, following Eq. (4.10), that the thick-film limit of the ripplons is a capillary-wave spectrum, $\omega^2 = \sigma q^3/\rho_0$. Then in this regime, the ripplon contributions to the thermodynamic properties are[52] ($x = \beta\hbar\omega$)

$$\rho_n = \beta\hbar^2 4\pi D \int_0^{\infty} dq\, q^3 e^x (e^x - 1)^{-2}\,, \tag{4.44}$$

$$\rho_n = 5\beta^{-5/3}\hbar^{-2/3}(\rho_0/\sigma)^{4/3}\Gamma(\tfrac{5}{3})\zeta(\tfrac{5}{3})/18\pi D\,,$$

$$c_s = 7 k_B^{7/3} T^{4/3} \hbar^{-4/3} (\rho_0/\sigma)^{2/3} \Gamma(\tfrac{7}{3})\zeta(\tfrac{7}{3})/3\pi D\,. \tag{4.45}$$

These expressions assume validity of the hydrodynamic expressions to large q and thus are probably not correct for $T \geq 0.5$ K. Note that even for very thick films these contributions dominate the bulk phonon term, which vary as $\rho_n \propto T^4$ and $c_s \propto T^3$, respectively.

V. CONCLUSIONS

Using the theory of quantum hydrodynamics we have given a detailed analysis of the elementary excitations and resultant thermodynamics of superfluid He^4 in restricted geometries of two types, cylindrical and planar. This analysis has considerably clarified the role of size effects in such systems, providing explicit criteria governing various regimes of film temperature and thickness. Further experiments, especially at low temperatures and, for the cylindrical case, in

more carefully controlled geometry, would provide valuable tests of quantum hydrodynamics applied to systems of reduced dimensionality.

The striking instability found in cylindrical pores has led to the suggestion that a new type of superfluidity, for two-dimensional He^3 systems on the inner surface of He^4 adsorbed in the pores, might be possible. It should be pointed out that this phenomenon, if it exists, would not depend critically on the details of pore geometry. Such an instability, and its associated soft modes leading to enhancement of the attractive part of the He^3-He^3 quasiparticle interaction, depends only on the competition between the substrate van der Waals force and the films' surface energy. Since this force will, by symmetry, vanish somewhere within any pore, the existence of the instability is rather independent of the details of pore shapes.

Finally, the instability and its associated metastability have led to a new explanation of the hysteresis observed in sorption isotherm measurements in porous media. Since our explanation depends on the assumption that the film be metastable along a portion of the adsorption curve, it could perhaps be tested by attempting to destroy the metastability.

ACKNOWLEDGMENTS

We are grateful to J. G. Dash for helpful comments and to J. D. Reppy and R. H. Tait for useful discussions and for providing us with data.

APPENDIX A

Here we sketch the calculation of the van der Waals potential inside a cylindrical pore. From (2.21) and the discussion following it, we have, taking into account the cylindrical symmetry,

$$U(a) = -\frac{6\alpha}{\pi}\int_R^\infty dr' r' \int_0^{2\pi} d\theta' \int_{-\infty}^{\infty} dz' \times[r'^2+z'^2+a^2-2ar'\cos\theta']^{-3} = -\frac{9\alpha}{\pi}\int_R^\infty dr' r' \int_0^{\pi} d\theta'[r'^2+a^2-2ar'\cos\theta']^{5/2}. \tag{A1}$$

But,[53] for $|b|<1$,

$$\int_0^\pi dx\,[1+2b\cos x+b^2]^{-\nu} = \pi F(\nu,\nu;1;b^2),$$

where F is a hypergeometric function. Hence (A1) becomes

$$U(a) = -\frac{9\pi\alpha}{2}\int_R^\infty dr\, r^{-4} F(\tfrac{5}{2},\tfrac{5}{2};1;(a/r)^2). \tag{A2}$$

Making the change of variables $z=(a/r)^2$, we write (A2) as

$$U(a) = -\frac{9\pi\alpha}{4a^3}\int_0^{y_2} dz\,\sqrt{z}\,F(\tfrac{5}{2},\tfrac{5}{2};1;z), \tag{A3}$$

where $y\equiv a/R$. Using the identity[54]

$$z^{1/2}F(\tfrac{5}{2},b;c;z) = \frac{2}{3}\frac{d}{dz}\left[z^{3/2}F(\tfrac{3}{2},b;c;z)\right],$$

the integral in (A3) is immediately done, yielding

$$U(a) = -(3\pi\alpha/2R^3)F(\tfrac{3}{2},\tfrac{5}{2};1;y^2), \tag{A4}$$

the result, (3.47), quoted in the text.

It is convenient to have an expression for the derivative of $U(a)$. Using the expression[55]

$$\frac{d}{dz}F(a,b;c;z) = \frac{ab}{c}F(a+1,b+1;c+1;z),$$

we find

$$g(a)\equiv\frac{-U'(a)}{m_4} = \frac{45\pi\alpha}{4R^4}\,yF(\tfrac{5}{2},\tfrac{7}{2};2;y^2). \tag{A5}$$

This can be written in the form[56]

$$g(a) = \frac{3\pi\alpha}{R^4}[1-y^2]^{5/2}P^1_{3/2}\left(\frac{1+y^2}{1-y^2}\right), \tag{A6}$$

where $P^1_{3/2}$ is an associated Legendre function.

To obtain explicit results for $g(a)$ we have numerically integrated the integral representation[57]

$$P^1_{3/2}(z) = \frac{5}{2\pi}\int_0^\pi [z+(z^2-1)^{1/2}\cos\varphi]^{3/2}\cos\varphi\, d\varphi. \tag{A7}$$

Further numerical integration yields $U(a)$. The limit of $g(a)$ for a near R is most easily found by using (A7). From the result, (3.48) is immediately obtained.

APPENDIX B: SUM FORMULA

Given a function $g(x)$ which vanishes at inifinity, the Euler-MacLaurin formula gives the relation between a sum and an integral in terms of derivatives of g at the lower limit[58]:

$$B\equiv\int_{x_1}^\infty dx\,g(x) = h[\tfrac{1}{2}g_1+g_2+g_3+\cdots] + \tfrac{1}{12}h^2g_1^{(1)} - \tfrac{1}{120}h^4g_1^{(3)} + h^6g_1^{(5)}/6!\,42+\cdots \tag{B1}$$

Here we treat the special case of $x_n=\frac{1}{2}nh$, where n is an odd integer, and use the notation

$$g_i\equiv g(x_i),\quad g_i^{(\nu)}\equiv\left.\frac{d^\nu g}{dx^\nu}\right|_{x=x_i}.$$

Our goal is to derive an equation differing from (B1) in that the lower limit of the integral is zero, the factor g_1 in brackets is multiplied by one rather than one half, and the derivatives of g are evaluated at $x=0$. We need the following equations:

$$B'\equiv\int_0^\infty dx\,g(x) = B+\int_0^{x_1} dx\,[g_1+g_1^{(1)}(x-x_1)+\tfrac{1}{2}g_1^{(2)}(x-x_1)^2+\cdots],$$

$$B' = B+\tfrac{1}{2}hg_1-\tfrac{1}{8}h^2g_1^{(1)}+\tfrac{1}{48}h^3g_1^{(2)}$$

$$-\tfrac{1}{384}h^4 g_1^{(3)}+\tfrac{1}{3840}h^5 g_1^{(4)}-h^6 g_1^{(5)}/5!(6)2^6+\cdots,$$

$$g_1^{(1)}=g_0^{(1)}+\tfrac{1}{2}hg_0^{(2)}+\tfrac{1}{8}h^2 g_0^{(3)}+\tfrac{1}{48}h^3 g_0^{(4)}+\tfrac{1}{384}h^4 g_0^{(5)}+\cdots,$$

$$g_1^{(2)}=g_0^{(2)}+\tfrac{1}{2}hg_0^{(3)}+\tfrac{1}{8}h^2 g_0^{(4)}+\tfrac{1}{48}h^3 g_0^{(5)}+\cdots,$$

$$g_1^{(3)}=g_0^{(3)}+\tfrac{1}{2}hg_0^{(4)}+\tfrac{1}{8}h^2 g_0^{(5)}+\cdots,$$

$$g_1^{(4)}=g_0^{(4)}+\tfrac{1}{2}hg_0^{(5)}+\cdots$$

Combining these with (B1), we obtain the desired result,

$$\sum_{\text{odd } i} g_i = h^{-1}\int_0^\infty dx\, g(x)+\tfrac{1}{24}hg_0^{(1)}-\tfrac{1}{5760}7h^3 g_0^{(3)}+31h^5 g_0^{(5)}/967\,680+\cdots. \qquad \text{(B2)}$$

---

*Research supported by National Science Foundation Grants # 11-5608 and GH-31650A-1 at the University of Washington and Ohio State University, respectively.

†Present address, Department of Physics, Pennsylvania State University, University Pa., 16802

[1]G. V. Chester, M. E. Fisher, and N. D. Mermin, Phys. Rev. 185, 760 (1969).

[2]J. A. Herb and J. G. Dash, Phys. Rev. Lett. 29, 846 (1972).

[3]J. H. Scholtz, E. O. McLean, and I. Rudnick, Phys. Rev. Lett. 32, 147 (1974).

[4]M. H. W. Chan, A. W. Yanof, and J. D. Reppy, Phys. Rev. Lett. 32, 1347 (1974).

[5]K. R. Atkins, Phys. Rev. 113, 962 (1959).

[6]K. A. Shapiro and I. Rudnick, Phys. Rev. 137, A1383 (1965).

[7]K. R. Atkins and I. Rudnick, in *Progress in Low Temperature Physics*, edited by C. J. Gorter (North-Holland, Amsterdam, 1970), Vol. VI.

[8]D. J. Bergman, Phys. Rev. 188, 370 (1969); A 3, 2058 (1971).

[9]A preliminary report on this work has already appeared. See M. W. Cole and W. F. Saam, Phys. Rev. Lett. 32, 985 (1974).

[10]M. Chester and L. C. Yang, Phys. Rev. Lett. 31, 1377 (1973).

[11]The present model has been given some theoretical justification by a calculation of D. J. Amit [J. Low Temp. Phys. 3, 645 (1970)] within the Hartree liquid approximation.

[12]D. O. Edwards (private communication). In any case, if the superfluid density is reduced because of healing of an order parameter near boundaries, one can make a subtraction to account for the effect.

[13]See, E.g., I. M. Khalatnikov, *An Introduction to the Theory of Superfluidity* (Benjamin, New York, 1965).

[14]See, e.g., L. D. Landau and E. M. Lifshitz, *Statistical Physics* (Pergamon, London, 1958), paragraph 25.

[15]See, e.g., L. D. Landau and E. M. Lifshitz, *Fluid Mechanics* (Pergamon, London, 1959), Chap. VII.

[16]We assume σ to be independent of curvature. This has been justified within the context of model calculations by T. C. Padmore and M. W. Cole [Phys. Rev. A 9, 802 (1974)], and C. Ebner and W. F. Saam (unpublished).

[17]This has been carried out in detail by one of us [W. F. S. (unpublished)] for the case of a planar free surface bounding a semi-infinite system. We simply assume that all aspects of this calculation, including completeness proofs, can be carried through for more general geometries.

[18]W. F. Saam, Phys. Rev. A 8, 1918 (1973).

[19]I. E. Dzyaloshinski, E. M. Lifshitz, and L. P. Pitaevski, Adv. Phys. 10, 165 (1961).

[20]E. S. Sabisky and C. H. Anderson, Phys. Rev. A 7, 790 (1973).

[21]E. S. Sabisky and C. H. Anderson, Phys. Rev. Lett. 30, 1122 (1973).

[22]D. F. Brewer, J. Low Temp. Phys. 3, 205 (1970).

[23]S. Brunauer, P. H. Emmett, and E. Teller, J. Am. Chem. Soc. 60, 309 (1938).

[24]See, e.g., S. J. Gregg and K. S. W. Sing, *Adsorption, Surface Area, and Porosity* (Academic, New York, 1967), Chaps. 3 and 4.

[25]D. F. Brewer and D. C. Champeney, Proc. Phys. Soc. Lond. 79, 855 (1962).

[26]The superfluid transition temperature depends upon the geometrical details. See, e.g., Ref. 4.

[27]Except when otherwise noted, all properties of Bessel functions used in this work may be found in the article by F. J. W. Oliver, *Handbook of Mathematical Functions*, edited by M. Abramowitz and I. A. Stegun (Dover, N. Y., 1965), Sec. 9.

[28]R. H. Tait and J. D. Reppy (unpublished).

[29]The fourth-sound experiments (which yield ρ_n) have been carried out by H. Hall, C. Kiewiet, and J. Reppy [J. Reppy, (private communication)]. The third-sound results, from which ρ_n for partially filled pores is obtained, are reported by D. Bishop, J. Parpia, A. W. Yanof, and J. Reppy [Bull. Am. Phys. Soc. 19, 435 (1974)].

[30]A. W. Yanof and J. D. Reppy (unpublished); J. B. Mehl and W. Zimmerman, Jr., Phys. Rev. 167, 214 (1968).

[31]An instability somewhat similar in nature is the well-known classical liquid jet instability. See, e.g., V. G. Levich, *Physiochemical Hydrodynamics* (Prentice-Hall, Englewood Cliffs, N. J., 1962), pp. 626–634.

[32]The γ and ζ functions have the numerical values $\Gamma(\frac{3}{2})=\frac{1}{2}\sqrt{\pi}=0.8862$, $\zeta(\frac{3}{2})=2.612$.

[33]See, e.g., Ref. 19, or Ref. 14, Chap. 12. A simple alternative derivation of (3.24), making the $T=0$ approximation at the beginning follows immediately from the requirement that

$$\frac{\partial\mu}{\partial N}=2\pi L\vartheta^2\left[a\sigma+\frac{\rho_0}{m_4}\int_a^R rU(r)\,dr\right]\Big/\vartheta N^2$$

be positive (L is the pore length).

[34]This is a slight generalization of the Kelvin equations for adsorption phenomena. See, e.g., S. J. Gregg and K. S. W. Sing, *Adsorption, Surface Area and Porosity* (Academic, New York, 1967).

[35]See, e.g., J. J. Stoker, *Differential Geometry* (Wiley, New York, 1969), Chap. IV.

[36]Due to some small numerical errors, the y_m's in Ref. 9 are slightly smaller than those shown in Fig. 3.

[37]See J. R. Eckardt, D. W. Edwards, P. P. Fatouros, F. M. Gasparini, and Y. S. Shen, Phys. Rev. Lett. 32, 706 (1974), and references quoted therein.

[38]J. Bardeen, G. Baym, and D. Pines, Phys. Rev. 156, 207 (1966).

[39]This assumes that the shorter range, direct part of the interaction is not much altered in going from the planar to the cylindrical surface. Estimates of superfluid transition temperatures are notoriously unreliable, and we refrain from attempting to make one here.
[40]M. W. Cole, Phys. Rev. A 1, 1838 (1970).
[41]B. L. Blackford, Phys. Rev. Lett. 28, 414 (1972).
[42]The thickness was calculated from the theory of Ref. 19. A small modification was made to account for the inhomogeneous region near the substrate.
[43]Data at higher temperatures are available. See Ref. 4 and D. C. Hickernell, E. O. McLean, and O. E. Vilches, J. Low Temp. Phys. 13, 241 (1973).
[44]L. S. Reut and I. Z. Fisher, Zh. Eksp. Teor. Fiz. 60, 1814 (1971) [Sov. Phys.-JETP 33, 981 (1971)].
[45]D. O. Edwards, J. R. Eckhardt, and F. M. Gasparini, Phys. Rev. A 9, 2070 (1974).
[46]Spectra without minima and which fit the data of Ref. 45 can be found. D.O. Edwards (private communication).
[47]James R. Eckhardt, Ph.D. thesis (Ohio State University, 1973) (unpublished).
[48]T. C. Padmore, Phys. Rev. Lett. 32, 826 (1974).
[49]R. P. Feynman and M. Cohen, Phys. Rev. 102, 1189 (1956).
[50]T. C. Padmore and G. Chester, Phys. Rev. A 9, 1725 (1974).
[51]M. Bretz, Phys. Rev. Lett. 31, 1447 (1973).
[52]An expression for the energy was previously derived by K. R. Atkins, Can. J. Phys. 31, 1165 (1953).
[53]I. S. Gradshteyn and I. M. Ryzhik, *Table of Integrals, Series, and Products* (Academic, New York, 1965), p. 384.
[54]*Handbook of Mathematical Functions*, edited by M. Abramowitz and I. Stegun (Dover, New York, 1965), Eq. 15.2.3.
[55]Reference 54, Eq. 15.2.1.
[56]We use $F(a,b;c;z)=F(b,a;c;z)$ and Eqs. 15.4.14, 8.2.1, and 8.2.5 of Ref. 54 in succession.
[57]A. Erdélyi, W. Magnus, and F. Oberhettinger, *Higher Transcendental Functions* (McGraw-Hill, New York, 1969), Vol. 1, p. 157, Eq. (16).
[58]H. Margenau and G. M. Murphy, *The Mathematics of Physics and Chemistry* (Van Nostrand, Princeton, N. J., 1956), p. 474.